PHILOSOPHICAL TRANSACTIONS OF THE ROYAL SOCIETY A MATHEMATICAL, PHYSICAL & ENGINEERING SCIENCES

Infrared spectroscopy of small-molecule endofullerenes

T. Rõõm, L. Peedu, Min Ge, D. Hüvonen, U. Nagel, Shufeng Ye, Minzhong Xu, Z. Bacic, S. Mamone, M. H. Levitt, M. Carravetta, J.Y.-C. Chen, Xuegong Lei, N. J. Turro, Y. Murata and K. Komatsu

Phil. Trans. R. Soc. A 2013 **371**, 20110631, published 5 August 2013

PHILOSOPHICAL TRANSACTIONS OF THE ROYAL SOCIETY A

rsta.royalsocietypublishing.org

Research

Cite this article: Rõõm T, Peedu L, Ge M, Hüvonen D, Nagel U, Ye S, Xu M, Bačić Z, Mamone S, Levitt MH, Carravetta M, Chen JYC, Lei X, Turro NJ, Murata Y, Komatsu K. 2013 Infrared spectroscopy of small-molecule endofullerenes. Phil Trans R Soc A 371: 20110631.
http://dx.doi.org/10.1098/rsta.2011.0631

One contribution of 13 to a Theo Murphy Meeting Issue 'Nanolaboratories: physics and chemistry of small-molecule endofullerenes'.

Subject Areas:
optics, atomic and molecular physics

Keywords:
endohedral, fullerene, *para* and *ortho* hydrogen, infrared

Author for correspondence:
T. Rõõm
e-mail: toomas.room@kbfi.ee

Infrared spectroscopy of small-molecule endofullerenes

T. Rõõm[1], L. Peedu[1], Min Ge[1], D. Hüvonen[1], U. Nagel[1], Shufeng Ye[2], Minzhong Xu[2], Z. Bačić[2], S. Mamone[3], M. H. Levitt[3], M. Carravetta[3], J. Y.-C. Chen[4], Xuegong Lei[4], N. J. Turro[4,†], Y. Murata[5] and K. Komatsu[5]

[1]National Institute of Chemical Physics and Biophysics, Akadeemia tee 23, 12618 Tallinn, Estonia
[2]Department of Chemistry, New York University, New York, NY 10003, USA
[3]School of Chemistry, University of Southampton, Southampton SO17 1BJ, UK
[4]Department of Chemistry, Columbia University, New York, NY 10027, USA
[5]Institute for Chemical Research, Kyoto University, Kyoto 611-0011, Japan

Hydrogen is one of the few molecules that has been incarcerated in the molecular cage of C_{60} to form the endohedral supramolecular complex $H_2@C_{60}$. In this confinement, hydrogen acquires new properties. Its translation motion, within the C_{60} cavity, becomes quantized, is correlated with its rotation and breaks inversion symmetry that induces infrared (IR) activity of H_2. We apply IR spectroscopy to study the dynamics of hydrogen isotopologues H_2, D_2 and HD incarcerated in C_{60}. The translation and rotation modes appear as side bands to the hydrogen vibration mode in the mid-IR part of the absorption spectrum. Because of the large mass difference of hydrogen and C_{60} and the high symmetry of C_{60} the problem is almost identical to a vibrating rotor moving in a three-dimensional spherical potential. We derive potential, rotation, vibration and dipole moment parameters from the analysis of the IR absorption spectra. Our results were used to derive the parameters

[†]Deceased 24 November 2012.

Royal Society Publishing
Informing the science of the future

of a pairwise additive five-dimensional potential energy surface for $H_2@C_{60}$. The same parameters were used to predict H_2 energies inside C_{70}. We compare the predicted energies and the low-temperature IR absorption spectra of $H_2@C_{70}$.

1. Introduction

A small cavity inside the fullerene cage is a potential site for trapping atoms and has attracted the attention of scientists from the moment of discovery of C_{60} [1]. The demonstration of formation of $La@C_{60}$ after laser bombardment of La-impregnated graphite was immediate [2]. Since then the field of studies of endohedral fullerenes has been expanding. Endohedral fullerenes with noble gas (He and Ne [3]; Ar, Kr, Xe [4]), nitrogen [5] or phosphorus [6] atoms and with metal clusters [7] are made under extreme conditions using arc discharge, ion bombardment or high-pressure and high-temperature treatment.

Extreme methods are not suitable for encapsulation of small molecules. A different approach, 'chemical surgery', was applied by Rubin [8] when he made the first open-cage fullerene with an orifice large enough to load it with ^3He or H_2 using less extreme temperature and pressure [9]. Soon Murata *et al*. [10] synthesized another open-cage derivative of C_{60} and achieved 100% yield in filling with H_2. Subsequently, the generation of a closed-cage $H_2@C_{60}$ was observed in the process of matrix-assisted laser desorption/ionization time-of-flight mass spectrometry analysis of this open-cage complex. Chemical methods were developed to close open-cage fullerenes and $H_2@C_{60}$ was produced in milligram quantities [11,12]. To accommodate two hydrogen molecules a cavity larger than C_{60} was needed. Two H_2 were trapped in open-cage C_{70} with a yield of 3 : 97 in favour of species with one H_2 per cage [13]. The restoration of the closed cage retains approximately the same ratio of $(H_2)_2@C_{70}$ to $H_2@C_{70}$ [14]. Molecules other than hydrogen trapped in open-cage fullerenes are carbon monoxide [15], water [16,17], ammonia [18] and methane [19]. Recently, Kurotobi & Murata [20] succeeded in closing one of them and making the first closed-cage endohedral complex with a trapped polar molecule, $H_2O@C_{60}$. The rotational modes of endohedral water were observed by inelastic neutron scattering (INS), far infrared (far-IR) and nuclear magnetic resonance (NMR) at cryogenic temperatures [21].

To date, $H_2@C_{60}$ has been the most studied small-molecule endofullerene. The inhomogeneous distribution of interaction parameters is expected to be small, mainly because of the crystal field effects in solid $H_2@C_{60}$. The $H_2@C_{60}$ is a stable complex and can survive a short period of heating up to 500°C under vacuum [12]. These properties make $H_2@C_{60}$ appealing for spectroscopic and theoretical investigations of interactions between the molecular hydrogen and carbon nanosurfaces.

Three spectroscopic techniques—NMR, INS and infrared (IR)—have been used to study endohedral hydrogen. NMR studies cover spin lattice relaxation rates of $H_2@C_{60}$ in organic solvents [22,23], and in the presence of paramagnetic relaxants [24,25]. NMR was used to follow the *ortho–para* conversion in $H_2@C_{60}$ in the presence of molecular oxygen at 77 K [26] or upon photoexcitation of a C_{70} triplet state [27]. NMR study of micro-crystalline $H_2@C_{60}$ samples at cryogenic temperatures shows splitting of the $J = 1$ rotational state [28,29], a sign of the symmetry reduction from the icosahedral symmetry in the solid phase. Similarly, splitting of the ground *ortho* state was deduced from the heat capacity measurements [30].

An overview of the low-temperature NMR, INS and IR work on $H_2@C_{60}$ is given by Mamone *et al.* [31]. The first IR study of $H_2@C_{60}$ was limited to 6 K [32]. The translational and rotational transitions appeared as sidebands to the hydrogen molecule bond-stretching vibrational transition, $v = 0 \rightarrow 1$, in the mid-IR spectral range. The direct translational and rotational transitions were not observed in the far-IR below 200 cm^{-1} [33]. The extension of IR studies to higher temperature made it possible to probe the hydrogen–C_{60} interaction potential

in the ground $v=0$ and first excited $v=1$ vibrational states and a whole range of hydrogen isotopologues H_2, D_2 and HD were studied [33,34]. The isotope effects and translation–rotation coupling were also studied by INS in $H_2@C_{60}$ and $HD@C_{60}$ [35]. The translational and rotational energies of $H_2@C_{60}$ and $HD@C_{60}$ in the $v=0$ state determined by IR spectroscopy are consistent with the low-temperature INS results [35]. There are no Raman data on $H_2@C_{60}$, except a report on H_2 inside an open-cage fullerene [36].

In this paper, we will review the IR studies of hydrogen isotopologues in C_{60} and present the analysis of IR low-temperature spectra of $H_2@C_{70}$. The far-IR properties of $H_2O@C_{60}$ will not be reviewed here [21].

2. Theory

Quantum statistics plays an important role in the dihydrogen wave function symmetry and has a pronounced effect on the rotation of the hydrogen molecule [37]. The symmetry relative to the interchange of two protons dictates that there are two forms of molecular hydrogen, called *para*- and *ortho*-H_2. The two proton spins ($I_p=\frac{1}{2}$) are in the antisymmetric $I=0$ total nuclear spin state in *para*-H_2 and in the symmetric $I=1$ state in *ortho*-H_2. Even rotational quantum numbers J are allowed for *para*-H_2 and odd J for *ortho*-H_2. The nucleus of D is a boson, nuclear spin $I_d=1$. Thus, the rotational state with an even quantum number J has D_2 in the state where the total nuclear spin of D_2 is either zero or two, $I=0,2$. This is called *ortho*-D_2, while *para*-D_2 has the total nuclear spin $I=1$ and odd J values.

The ground rotational state of a homonuclear diatomic molecule with the total nuclear spin $I=1$ is the $J=1$ state. This $J=1$ rotational state is $118\,\mathrm{cm}^{-1}$ for H_2, and $58\,\mathrm{cm}^{-1}$ for D_2, above the rotational ground state $J=0$ of even-I species. A thermal transition $J=1\rightarrow 0$ must be accompanied by a change in the total nuclear spin of the molecule, a process of very low probability. The time constant of thermal relaxation between the *ortho* and the *para* manifolds is very long and the room temperature *ortho–para* ratio is maintained even at cryogenic temperatures. The equilibrium distribution of H_2 nuclear spin isomers is $n_o/n_p=3$ and of D_2 is $n_o/n_p=2$ at room temperature. To change the total nuclear spin of a molecule the two nuclei must experience different magnetic fields. The *ortho–para* conversion can be activated by using a paramagnetic centre as a source of the magnetic field gradient. The equilibrium $n_o/n_p=1.0$ is reached at 77 K by dispersing $H_2@C_{60}$ on a zeolite surface and exposing it to molecular oxygen, which acts like a spin catalyst [38]. There are no *ortho* and *para* species for HD. All rotational levels of HD are in thermal equilibrium and there is one rotational ground state, $J=0$.

Quantum chemistry calculations are challenging for a hydrogen molecule in a weak van der Waals interaction with a large fullerene molecule. The availability of experimental data on endohedral H_2 has stimulated theoretical work in this direction. Theoretical investigations currently cover the calculations of rotation–translation energies of hydrogen isotopologues in C_{60} [39,40] and H_2 in C_{70} [41], and the stability of C_{60} or C_{70} with one or more incarcerated H_2 [42,43]. Empirical parameters of the Morse potential between H–H and contact Dirac interaction between H–C were adjusted [44], and the density-fitting local Møller–Plesset theory was tested [45] using the experimental H_2 vibrational frequency inside C_{60}. Classical molecular dynamics and density functional theory have been combined to reproduce accurately the NMR chemical shift of ^1H in $H_2@C_{60}$ [46].

Both the hydrogen molecule and fullerene have closed-shell electronic structures and therefore the interaction between them is the van der Waals interaction. This simplicity makes $H_2@C_{60}$ ideal for the studies of non-covalent bondings between H_2 and carbon nanosurfaces, the knowledge needed for the design of carbon-based hydrogen storage materials. The high icosahedral symmetry of the C_{60} cavity is close to spherical; therefore, $H_2@C_{60}$ represents a textbook example of a body moving in a spherical potential well [47,48]. In addition, H_2 rotates around its centre of mass. H_2 is not spherical and therefore its interaction with the walls of the cavity depends on its orientation, which leads to the coupling between translational and rotational motion [49]. If the translational and the rotational motions are coupled then in the spherical potential the conserved

angular momentum is the sum of translational and rotational angular momenta [39,50]. $H_2@C_{60}$ is a rare example in which the quantum dynamics of a diatomic rotor in a confined environment can be studied. Another, but with limited degrees of freedom, interesting example related to the fullerenes is the quantum rotor C_2 in a metallofullerene $C_2@Sc_2C_{84}$ [51,52]. The two scandium atoms limit the translational motion and fix the rotational axis of C_2 relative to the fullerene cage. At low temperature, the rotation of C_2 is hindered because it has a small rotational constant and is therefore more susceptible to the corrugations of the carbon surface. H_2 provides examples of two-dimensional rotors, such as H_2 on a Cu surface [53] or H_2 in intercalated graphite [54].

High-pressure loading of solid C_{60} creates interstitial H_2. Exohedral H_2 has been studied by IR [55,56], INS [57,58], NMR [59,60] and Raman [61] spectroscopies. Hydrogen is trapped in an interstitial site of octahedral symmetry and theory predicts translation–rotation coupling [50,62]. However, broadening of experimental lines has prohibited accurate determination of the H_2–C_{60} interaction potential.

The observed IR spectra of hydrogen encapsulated in C_{60} consist of several absorption lines. We construct a model Hamiltonian and a dipole moment operator with few adjustable parameters to describe accurately the position and intensity of such a multi-line spectrum.

(a) Diatomic molecule in a spherical potential well

To describe the motion of a hydrogen molecule inside C_{60}, we use the following model. The C_{60} is considered to be rigid, its centre of mass is not moving and also does not rotate. We treat $H_2@C_{60}$ as an isolated molecular complex and approximate the true icosahedral symmetry of an isolated C_{60} with spherical symmetry. It means that, in this approximation, H_2 moves in a rigid spherically symmetric bounding potential provided by the cavity of C_{60}. Besides the translational movement inside C_{60} the hydrogen molecule has its internal degrees of freedom, vibration and rotation of two nuclei relative to its centre of mass. There are no coupling terms between *ortho* and *para* states in our model Hamiltonian.

The theoretical work of Olthof *et al.* [63] is a comprehensive description of the dynamics of a loosely bound molecule inside C_{60}. Olthof *et al.* [63] model the intermolecular potential as a sum of atom–atom potentials and expand it in spherical harmonics. They determined the radial part of the wave function with a discrete variable representation method. The radial part of the wave function in our approach is given by algebraic functions, which are solutions of the three-dimensional spherical oscillator [47,48,64]. The advantage is that matrix elements are calculated in algebraic form, avoiding time-consuming numerical integration.

The position and orientation of the H_2 molecule is given by spherical coordinates $\mathbf{R} = \{R, \Omega\}$, $\Omega = \{\Theta, \Phi\}$ and $\mathbf{s} = \{s, \Omega_s\}$, $\Omega_s = \{\theta, \phi\}$, where $\mathbf{R}$ is the vector from the centre of the C_{60} cage to the centre of mass of H_2 and $\mathbf{s}$ is the internuclear H–H vector. The centre of mass translational motion of H_2 is given by eigenfunctions of the isotropic three-dimensional harmonic oscillator [48,64]

$$\Psi^{v}_{NLM_L}(R, \Omega) = \psi^{v}_{NL}(R)\, Y_{LM_L}(\Omega), \tag{2.1}$$

where ψ^{v}_{NL} is the radial wave function and Y_{LM_L} is the spherical harmonic. The size of the H_2 molecule depends on its vibrational state $|v\rangle$. Therefore both the bounding potential and $\psi^{v}_{NL}(R)$ depend on the vibrational quantum number v. The translational quantum numbers are $N = 0, 1, 2, \ldots$. The orbital angular momentum quantum number takes values $L = N, N-2, \ldots, 1$ or 0, depending on the parity of N, and the azimuthal quantum number is $M_L = -L, -L+1, \ldots, L$. The rotational wave functions, defined by the rotational quantum numbers $J = 0, 1, \ldots$ and $M_J = -J, -J+1, \ldots, J$, are given by the spherical harmonics $Y_{JM_J}(\theta, \phi)$.

We use bipolar spherical harmonics with overall spherical rank Λ and component M_Λ

$$F^{LJ}_{\Lambda M_\Lambda}(\Omega, \Omega_s) = \sum_{M_L, M_J} C^{\Lambda M_\Lambda}_{LM_L JM_J} Y_{LM_L}(\Omega) Y_{JM_J}(\Omega_s), \tag{2.2}$$

where $\mathcal{C}$ are the Clebsch–Gordan coefficients [64]. Then the full wave function describing the motion of the H_2 molecule is

$$|vJNL\Lambda M_\Lambda\rangle = \psi_v^{\mathrm{vib}}(s)\psi_{NL}^{v}(R)F_{\Lambda M_\Lambda}^{LJ}(\Omega,\Omega_s), \tag{2.3}$$

where $\psi_v^{\mathrm{vib}}(s) \equiv |v\rangle$ is the vibrational wave function with the quantum number v.

The Hamiltonian $\mathcal{H}$ for the trapped molecule includes coupling terms between vibrational, translational and rotational motion. For simplicity, we neglect all matrix elements non-diagonal in v and introduce a parametric dependence on v,

$$\mathcal{H} = {}^{v}\mathcal{H}^{\mathrm{vib-rot}} + \frac{p^2}{2m} + {}^{v}V(R,\Omega,\Omega_s), \tag{2.4}$$

where ${}^{v}\mathcal{H}^{\mathrm{vib-rot}}$ is the vibration–rotation Hamiltonian, p is the molecular momentum operator and m is the molecular mass of the diatomic molecule. ${}^{v}V = \langle v|V(R,s,\Omega,\Omega_s)|v\rangle$ is the potential energy of the hydrogen molecule in the vibrational state $\psi_v^{\mathrm{vib}}(s)$. The vibration–rotation Hamiltonian ${}^{v}\mathcal{H}^{\mathrm{vib-rot}}$ is diagonal in the basis set $|vJNL\Lambda M_\Lambda\rangle$ with eigenvalues given by

$${}^{v}E_J^{\mathrm{vib-rot}} = \hbar\omega_0(v+\tfrac{1}{2}) + B_rJ(J+1), \tag{2.5}$$

$B_r = B_e - \alpha_e(v+\frac{1}{2}) - D_eJ(J+1)$, where ω_0 is the fundamental vibrational frequency, α_e is the anharmonic correction and D_e is the centrifugal correction to the rotational constant B_e [65,66].

We start from the general expansion of the potential in multi-poles,

$${}^{v}V(R,\Omega,\Omega_s) = \sum_{l,j,\lambda,m_\lambda} {}^{v}V_{\lambda m_\lambda}^{lj}(R)F_{\lambda m_\lambda}^{lj}(\Omega,\Omega_s), \tag{2.6}$$

and expand the radial part of potential ${}^{v}V_{\lambda m_\lambda}^{lj}(R)$ in powers of R

$${}^{v}V_{\lambda m_\lambda}^{lj}(R) = \sum_{n} {}^{v}V_{\lambda m_\lambda}^{ljn}R^n, \tag{2.7}$$

where $n \geq l$ and the parities of l and n are the same.

$V(\mathbf{R},\mathbf{s})$ is a scalar and transforms under fully symmetric representation A_g of the symmetry group I_h. The spherical harmonics $\lambda = 0, 6, 10, \ldots$ transform as A_g of the symmetry group I_h [67]. We use fully spherical approximation of the potential, $\lambda = 0$. Because $\lambda = 0$ and $\lambda = |l-j|, |l-j|+1, \ldots, l+j$ it must be that $l = j$.

The total potential is

$$\begin{aligned} {}^{v}V = {}&{}^{v}V_{00}^{000}F_{00}^{00} + ({}^{v}V_{00}^{002}R^2 + {}^{v}V_{00}^{004}R^4)F_{00}^{00} \\ &+ ({}^{v}V_{00}^{111}R + {}^{v}V_{00}^{113}R^3)F_{00}^{11} + ({}^{v}V_{00}^{222}R^2 + {}^{v}V_{00}^{224}R^4)F_{00}^{22}, \end{aligned} \tag{2.8}$$

if we limit our expansion to $j = l = 2$ and $n = 4$. The odd-j terms are not allowed by symmetry for H_2 and D_2 and thus the coefficients ${}^{v}V_{00}^{111}$ and ${}^{v}V_{00}^{113}$ are zero for homonuclear diatomic molecules.

If we set the constant off-set ${}^{v}V_{00}^{000}F_{00}^{00}$ to zero and write the perturbation part as

$${}^{v}V' = {}^{v}V_{00}^{004}R^4F_{00}^{00} + ({}^{v}V_{00}^{111}R + {}^{v}V_{00}^{113}R^3)F_{00}^{11} + ({}^{v}V_{00}^{222}R^2 + {}^{v}V_{00}^{224}R^4)F_{00}^{22}, \tag{2.9}$$

and the isotropic harmonic term as ${}^{v}V^0 = {}^{v}V_{00}^{002}R^2F_{00}^{00}$, then the total Hamiltonian reads

$$\mathcal{H} = {}^{v}\mathcal{H}^{\mathrm{vib-rot}} + \frac{p^2}{2m} + {}^{v}V^0 + {}^{v}V'. \tag{2.10}$$

The unperturbed Hamiltonian eigenvalues in the basis $|vJNL\Lambda M_\Lambda\rangle$ are

$$E^0_{vJNL\Lambda M_\Lambda} = {}^{v}E_J^{\mathrm{vib-rot}} + \hbar\,{}^{v}\omega_0^{\mathrm{T}}(N+\tfrac{3}{2}), \tag{2.11}$$

where ${}^{v}\omega_0^{\mathrm{T}} = ({}^{v}V_{00}^{002}/(2\pi m))^{1/2}$ is the frequency for translational oscillations within the cavity.

The meaning of different parts of the perturbation is explained by their influence on the energy levels of a harmonic three-dimensional spherical oscillator (table 1). The translation–rotation coupling term ${}^{v}V_{00}^{222}$ splits the energy of the $|vJNL\Lambda\rangle$ state into levels with different

Table 1. Translation–rotation energies of a three-dimensional spherical oscillator $\langle {}^{v}JNL\Lambda|\mathcal{H} - {}^{v}\mathcal{H}^{\mathrm{vib-rot}}|{}^{v}JNL\Lambda\rangle$ for a perturbation given by equation (2.9) and $\mathcal{H}$ by equation (2.10) for a few lower states. Here, ${}^{v}\Delta^{004} = (1/{}^{v}\beta)(15/8)({}^{v}V_{00}^{004}/{}^{v}V_{00}^{002})$, ${}^{v}\Delta^{222} = (\sqrt{5}/20)({}^{v}V_{00}^{222}/{}^{v}V_{00}^{002})$, ${}^{v}\Delta^{224} = (1/{}^{v}\beta)(7/8\sqrt{5})({}^{v}V_{00}^{224}/{}^{v}V_{00}^{002})$ and for ${}^{v}\beta$ see equation (2.12).

$JNL\Lambda$	$\langle {}^{v}JNL\Lambda\|\mathcal{H} - {}^{v}\mathcal{H}^{\mathrm{vib-rot}}\|{}^{v}JNL\Lambda\rangle$
0000	$\hbar{}^{v}\omega_0^{\mathrm{T}}[\frac{3}{2} + {}^{v}\Delta^{004}]$
1001	$\hbar{}^{v}\omega_0^{\mathrm{T}}[\frac{3}{2} + {}^{v}\Delta^{004}]$
0111	$\hbar{}^{v}\omega_0^{\mathrm{T}}[\frac{5}{2} + \frac{7}{3}{}^{v}\Delta^{004}]$
1110	$\hbar{}^{v}\omega_0^{\mathrm{T}}[\frac{5}{2} + \frac{7}{3}{}^{v}\Delta^{004} + 10({}^{v}\Delta^{222} + {}^{v}\Delta^{224})]$
1111	$\hbar{}^{v}\omega_0^{\mathrm{T}}[\frac{5}{2} + \frac{7}{3}{}^{v}\Delta^{004} - 5({}^{v}\Delta^{222} + {}^{v}\Delta^{224})]$
1112	$\hbar{}^{v}\omega_0^{\mathrm{T}}[\frac{5}{2} + \frac{7}{3}{}^{v}\Delta^{004} + 1({}^{v}\Delta^{222} + {}^{v}\Delta^{224})]$
2111	$\hbar{}^{v}\omega_0^{\mathrm{T}}[\frac{5}{2} + \frac{7}{3}{}^{v}\Delta^{004} + 5({}^{v}\Delta^{222} + {}^{v}\Delta^{224})]$
2112	$\hbar{}^{v}\omega_0^{\mathrm{T}}[\frac{5}{2} + \frac{7}{3}{}^{v}\Delta^{004} - 5({}^{v}\Delta^{222} + {}^{v}\Delta^{224})]$
2113	$\hbar{}^{v}\omega_0^{\mathrm{T}}[\frac{5}{2} + \frac{7}{3}{}^{v}\Delta^{004} + \frac{10}{7}({}^{v}\Delta^{222} + {}^{v}\Delta^{224})]$
0200	$\hbar{}^{v}\omega_0^{\mathrm{T}}[\frac{7}{2} + 5{}^{v}\Delta^{004}]$
0222	$\hbar{}^{v}\omega_0^{\mathrm{T}}[\frac{7}{2} + \frac{21}{5}{}^{v}\Delta^{004}]$
1201	$\hbar{}^{v}\omega_0^{\mathrm{T}}[\frac{7}{2} + 5{}^{v}\Delta^{004}]$
1221	$\hbar{}^{v}\omega_0^{\mathrm{T}}[\frac{7}{2} + \frac{21}{5}{}^{v}\Delta^{004} + 7({}^{v}\Delta^{222} + \frac{9}{7}{}^{v}\Delta^{224})]$
1222	$\hbar{}^{v}\omega_0^{\mathrm{T}}[\frac{7}{2} + \frac{21}{5}{}^{v}\Delta^{004} - 7({}^{v}\Delta^{222} + \frac{9}{7}{}^{v}\Delta^{224})]$
1223	$\hbar{}^{v}\omega_0^{\mathrm{T}}[\frac{7}{2} + \frac{21}{5}{}^{v}\Delta^{004} + 2({}^{v}\Delta^{222} + \frac{9}{7}{}^{v}\Delta^{224})]$

Λ, where $\Lambda = |L-J|, |L-J|+1, \ldots, L+J$. For example, the $N=L=J=1$ state is split into three levels with different total angular momentum $\Lambda = 0, 1, 2$. The ordering of levels depends on the sign of ${}^{v}V_{00}^{222}$. The anharmonic correction to translation–rotation coupling is ${}^{v}V_{00}^{224}$. If isotropic anharmonic correction ${}^{v}V_{00}^{004}$ is positive, the distance between energy levels increases with N and this correction is different for the levels with same N but different L. For example, for positive ${}^{v}V_{00}^{004}$ the $N=2, L=0$ level has higher energy than the $N=2, L=2$ level.

The length scale ${}^{v}\beta = m{}^{v}\omega_0^{\mathrm{T}}/\hbar$ (dimension m^{-2}) of the radial part of a three-dimensional spherical oscillator wave function is related to the expectation value of the centre of mass amplitude in state $|N\rangle$ as [47]

$$\langle N|R^2|N\rangle = {}^{v}\beta^{-2}\left(N+\frac{3}{2}\right) = \hbar\sqrt{\frac{2\pi}{m{}^{v}V_{00}^{002}}}\left(N+\frac{3}{2}\right). \tag{2.12}$$

Terms described by the translation–rotation coupling coefficients ${}^{v}V_{00}^{111}$ and ${}^{v}V_{00}^{113}$ do not appear in table 1 because the first-order correction to energies vanishes as the matrix element of F_{00}^{11} is zero if diagonal in L or J. These terms mix states with different N and J. For example, the first excited rotational state $J=1, N=0$ (expectation value of HD centre of mass is on the cage centre) has the state $J=0, N=1$ (expectation value of HD centre of mass is off the cage centre) mixed in [34]. The effect is that HD is forced to rotate about its geometric centre instead of its centre of mass.

It was found by the five-dimensional quantum mechanical calculation that the rotational quantum number J is almost a good quantum number for the homonuclear $H_2@C_{60}$ and $D_2@C_{60}$ and not for the heteronuclear $HD@C_{60}$ [40]. Indeed, ${}^{v}V_{00}^{22n}$ mixes states with different J for homonuclear species as well, but the effect is reduced compared with the effect of ${}^{v}V_{00}^{11n}$. In the former case, $J \pm 2$ and $L \pm 2$ are mixed, while in the latter case the $J \pm 1$ and $L \pm 1$ states that have a smaller energy separation are mixed.

The states with different Λ are not mixed in the spherical approximation, i.e. the total angular momentum $\Lambda = \mathbf{L} + \mathbf{J}$ is conserved and Λ is a good quantum number. The other consequence of the spherical symmetry is that the energy does not depend on M_Λ. Therefore, it is practical to use a reduced basis and reduced matrix elements [68] which are independent of M_Λ. This reduces the number of states by factor $2\Lambda + 1$ for each Λ.

(b) Model Hamiltonian of $H_2@C_{70}$

A spherical approximation of the potential of a molecule trapped in C_{70} would be an oversimplification because of the elongated shape of C_{70}. The symmetry of C_{70} is D_{5h}, the distance between the centres of two capping pentagons (z-direction) is 7.906 Å. The diameter of the equatorial xy plane is 7.180 Å [69], similar to the diameter of the icosahedral sphere of C_{60}, 7.113 Å [70]. The anisotropy of the potential of H_2 inside C_{70} is supported by the five-dimensional quantum mechanical calculation [41] that shows that the lowest translational excitation in the z-direction is 54 cm^{-1} and in the xy plane is 132 cm^{-1}, while in C_{60} it is 180 cm^{-1} and isotropic [33]. We derive from the IR spectra (see below) that the xy plane excitation energy is 151 cm^{-1}, somewhat larger than theoretically predicted.

Although the z-axis translational energy in C_{70} is three times less than in the icosahedral C_{60}, the effect of the C_{70} potential on the rotational motion is moderate. The splitting of the $J = 1$ state is 7 cm^{-1}, which is relatively small compared with the rotational energy 120 cm^{-1} in this state [41].

To analyse the IR spectra of $H_2@C_{70}$, we use a simplified Hamiltonian in which the translational energy is represented in the form of the sum of two oscillators, a one-dimensional linear and a two-dimensional circular oscillator, and we do not consider anharmonic corrections and the translation–rotation coupling.

The vibration–rotation energy

$$ {}^{v}E^{\mathrm{vib-rot}}_{JJ_z} = \hbar\,\omega_0(v + \tfrac{1}{2}) + B_r^{(v)} J(J+1) + {}^{v}\kappa(3J_z^2 - 2) \tag{2.13} $$

is the same as for $H_2@C_{60}$ except the last term, which accounts for the axial symmetry of the C_{70} potential with the rotational anisotropy parameter ${}^{v}\kappa$ [71]. For example, the three-fold degenerate $J = 1$ rotational state in I_h symmetry is split in D_{5h} symmetry and if ${}^{v}\kappa > 0$ the $J_z = 0$ state is $3\,{}^{v}\kappa$ below the twice degenerate $J_z = \pm 1$ rotational state.

The translational part is added to the vibration–rotation Hamiltonian, equation (2.13), and the total energy becomes

$$ E^0_{vJJ_z;nln_z} = {}^{v}E^{\mathrm{vib-rot}}_{JJ_z} + \hbar\,{}^{v}\omega^{\mathrm{T}}_{xy}(n+1) + \hbar\,{}^{v}\omega^{\mathrm{T}}_{z}(n_z + \tfrac{1}{2}). \tag{2.14} $$

Here, the translational energy is written as a sum of two oscillators, a linear oscillator along the z-axis with translational quantum $\hbar\,{}^{v}\omega^{\mathrm{T}}_{z}$ and a two-dimensional (circular) oscillator [48,64] in the xy plane with translational quantum $\hbar\,{}^{v}\omega^{\mathrm{T}}_{xy}$. Quantum numbers n_z and n are positive integers including zero and $l = n, n-2, \ldots, -n+2, -n$.

We will show below that the frequencies of z and xy translational modes, ${}^{1}\omega^{\mathrm{T}}_{z}$ and ${}^{1}\omega^{\mathrm{T}}_{xy}$, can be determined from the experimental data even though the translation–rotation coupling is not known. We take advantage of translation–rotation coupling being zero in the $J = 0$ rotational state. The complication arises from the fact that the potential is different in the initial and final states of the IR transitions, $v = 0$ and 1. However, this complication could be resolved if the energy of the fundamental vibrational transition $v = 0 \to 1$ (without change of n and n_z) is known.

The $\Delta J = 0$ transition from the *para*-H_2 ground state leads to two excitation energies in the IR spectrum, first for the z mode and second for the xy mode

$$ E^0_{100;001} - E^0_{000;000} = \hbar[\omega_0 + {}^{1}\omega^{\mathrm{T}}_{z} + ({}^{1}\omega^{\mathrm{T}}_{xy} - {}^{0}\omega^{\mathrm{T}}_{xy}) + \tfrac{1}{2}({}^{1}\omega^{\mathrm{T}}_{z} - {}^{0}\omega^{\mathrm{T}}_{z})] \tag{2.15} $$

and

$$ E^0_{100;110} - E^0_{000;000} = \hbar[\omega_0 + {}^{1}\omega^{\mathrm{T}}_{xy} + ({}^{1}\omega^{\mathrm{T}}_{xy} - {}^{0}\omega^{\mathrm{T}}_{xy}) + \tfrac{1}{2}({}^{1}\omega^{\mathrm{T}}_{z} - {}^{0}\omega^{\mathrm{T}}_{z})]. \tag{2.16} $$

Table 2. Classification of energy levels of H_2 inside the cage of C_{70} up to $J = 1$ and $n = n_z = 1$ by irreducible representations Γ_i of the symmetry group D_{5h}.

J	(nln_z)	Γ_i
0	(000)	A_1'
1	(000)	A_2'', E_1'
0	(001)	A_2''
1	(001)	A_1', E_1''
0	(110)	E_1'
1	(110)	A_1', A_2', E_2', E_1''

Defining the fundamental *para* transition energy as $E^0_{100;000} - E^0_{000;000} = \hbar[\omega_0 + ({}^1\omega^{\mathrm{T}}_{xy} - {}^0\omega^{\mathrm{T}}_{xy}) + \frac{1}{2}({}^1\omega^{\mathrm{T}}_{z} - {}^0\omega^{\mathrm{T}}_{z})]$, we may rewrite equations (2.15) and (2.16) as

$$\left.\begin{aligned} E^0_{100;001} - E^0_{000;000} &= \hbar\, {}^1\omega^{\mathrm{T}}_{z} + E^0_{100;000} - E^0_{000;000} \\ \text{and} \qquad E^0_{100;110} - E^0_{000;000} &= \hbar\, {}^1\omega^{\mathrm{T}}_{xy} + E^0_{100;000} - E^0_{000;000}. \end{aligned}\right\} \tag{2.17}$$

From these equations, translational frequencies in the excited $v = 1$ state, ${}^1\omega^{\mathrm{T}}_{z}$ and ${}^1\omega^{\mathrm{T}}_{xy}$, can be determined without knowing the translation–rotation coupling.

The classification of energy levels up to $J = 1$ and $n = n_z = 1$ by irreducible representations Γ_i of the symmetry group D_{5h} is given in table 2. We get the irreducible representations Γ_j: $L = 0 \to A_1'$ and $L = 1 \to A_2'' + E_1'$ by subducting the translational states represented by spherical harmonics Y_{LM_L} from the full rotational group $O(3)$ to the symmetry group D_{5h}. A_1' is the *para*-H_2 ground state, $n = l = n_z = 0$. The first excited state of the z mode is $n_z = 1$ and A_2''. The first excited state of the xy mode $n = l = 1$ is doubly degenerate E_1'. The full symmetry when translations and rotations are taken into account is $\Gamma_i = \Gamma_j \otimes \Gamma^{(J)}$. For example, the *ortho*-H_2 ground state, $J = 1$ and $(nln_z) = (000)$, is split into $J_z = 0$ (A_2'') and $J_z = \pm 1$ (E_1') (table 2).

(c) Induced dipole moment of hydrogen in a spherical environment

IR light is not absorbed by vibrations and rotations of isolated homonuclear diatomic molecules [65]. IR activity of H_2 is induced in the presence of intermolecular interactions, such as in the solid and liquid phases [72,73], in constrained environments [55,56,62,74], and in pressurized gases [75,76]. IR spectra of such systems are usually broad because of inhomogeneities in the system or because of random molecular collisions. As an exception, narrow lines are observed in semiconductor crystals [77] and solid hydrogen [78].

An overview of collision-induced dipoles in gases and gas mixtures is given in a book by Frommhold [79]. The confinement of the endohedral H_2 introduces two differences when compared with H_2 in the gas. *First*, the translational energy of H_2 is quantized. In the gas phase, it is a continuum starting from zero energy. *Second*, the variation of the distance between H_2 and the carbon atom is limited to the translational amplitude of H_2 in the confining potential. In the gas phase, the distance varies from infinity to the minimal distance given by the collision radius. The selection rule $\Delta N = \pm 1$ for the endohedral H_2 follows from these two conditions, as shown below.

Quantum mechanical calculations of induced dipoles are available for simple binary systems such as H_2–He, H_2–Ar and H_2–H_2. An extensive set of theoretical results for the H_2–He system associated with the roto-translation electric dipole transitions, both in the vibrational ground state $v = 0$ and accompanying the $v = 0 \to 1$ transition of the H_2 molecule, can be found in [80–84]. Related to the fullerene studies are calculations of the dipole moment of CO@C_{60} [63] and exohedral H_2 in solid C_{60} [62].

We express the induced part of the dipole moment as an interaction between a hydrogen molecule and C_{60}. Another approach was used by Ge *et al.* [33], who carried out a summation over 60 pair-wise induced dipole moments between H_2 and carbon atoms. The relation between two sets of parameters was given [34].

We write the expansion of the dipole moment from the vibrational state v to v' in bipolar spherical harmonics and in power series of R as

$$d_{v'v}(\mathbf{R}, \Omega_s) = \frac{4\pi}{\sqrt{3}} \sum_{l,j,n} {}^{v'v}A^{ljn}_{\lambda m_\lambda} R^n F^{lj}_{\lambda m_\lambda}(\Omega, \Omega_s). \tag{2.18}$$

This is similar to the expansion of the potential discussed above, except the dipole moment is a polar vector whereas the potential is a scalar. The dipole moment transforms according to the irreducible representation T_{1u} of the symmetry group I_h. The spherical harmonics of the order $\lambda = 1, 5, 7, \ldots$ transform according to T_{1u} of the symmetry group I_h [67]. We use $\lambda = 1$ and are interested in $v = 0 \to 1$ transitions. In spherical symmetry, it is sufficient to calculate one component of the dipole moment vector, $m_\lambda = 0$, and if we drop the explicit dependence of $d_{v'v}$ on v, v' and of ${}^{v'v}A^{ljn}_{\lambda m_\lambda}$ on λ, m_λ, the $m_\lambda = 0$ component of the dipole moment reads

$$d_0(\mathbf{R}, \Omega_s) = \frac{4\pi}{\sqrt{3}} \sum_{l,j,n} A^{ljn} R^n F^{lj}_{10}(\Omega, \Omega_s). \tag{2.19}$$

As $\lambda = |l - j|, |l - j| + 1, \ldots, l + j$ and $\lambda = 1$ it must be that $l = |j \pm 1|$. The possible combinations are $(lj) \in \{(01), (10), (12), (21), (23), \ldots\}$. If we restrict the expansion up to $n = l = 1$, we get

$$d_0(\mathbf{R}, \Omega_s) = \frac{4\pi}{\sqrt{3}} A^{010} F^{01}_{10} + \frac{4\pi}{\sqrt{3}} (A^{101} F^{10}_{10} + A^{121} F^{12}_{10}) R.$$

A^{010} is zero for homonuclear diatomic molecules H_2 and D_2. It is the sum of the HD permanent rotational dipole moment in the gas phase and the induced rotational dipole moment inside C_{60}. The selection rule is $\Delta N = 0, \Delta J = 0, \pm 1$, but $J = 0 \to 0$ is forbidden.

The expansion coefficients A^{101} and A^{121} are allowed by symmetry for both homo- and hetero-nuclear diatomic molecules. The expansion coefficient A^{101} describes the induced dipole moment that is independent of the orientation of the diatomic molecular axis $\mathbf{s}$, selection rule $\Delta N = 0, \pm 1, \Delta J = 0$, but $N = 0 \to 0$ is forbidden. A^{121} describes the induced dipole moment that depends on the orientation of $\mathbf{s}$, $\Delta N = 0, \pm 1$, $\Delta J = 0, \pm 2$, but $N = 0 \to 0$ and $J = 0 \to 0$ are both forbidden. All terms in equation (2.20) satisfy the selection rule $\Delta \Lambda = 0, \pm 1$, but $\Lambda = 0 \to 0$ is forbidden.

Although HD has a permanent rotational dipole moment, the induced dipole moment dominates inside C_{60} [34].

IR absorption line intensity [33] is proportional to the thermal population of the initial state. If the thermal relaxation between *para*-H_2 and *ortho*-H_2 is very slow we can define temperature-independent fractional *ortho* and *para* populations n_k of the total number of molecules $\mathcal{N}$, where $k = o, p$ selects *ortho*- or *para*-H_2. Then the probability that the initial state $|v_i J_i N_i L_i \Lambda_i M_{\Lambda_i}\rangle$ is populated is

$$p_i = n_k \frac{e^{-E_i/k_B T}}{\sum_j g_j e^{-E_j/k_B T}}, \tag{2.20}$$

where E_i is the energy of the initial state measured from the ground state $v = N = 0$ and j runs over all *para*- (or *ortho*-) H_2 states in the basis used. $g_j = 2\Lambda_j + 1$ is the degeneracy of the energy level E_j. Please note that g_i does not appear in the numerator because p_i is the population of an individual state $|v_i J_i N_i L_i \Lambda_i M_{\Lambda_i}\rangle$, although the reduced basis $|vJNL\Lambda\rangle$ is used. Hetero-nuclear HD has no *para* or *ortho* species and the coefficient n_k in equation (2.20) must be set to one, $n_k = 1$.

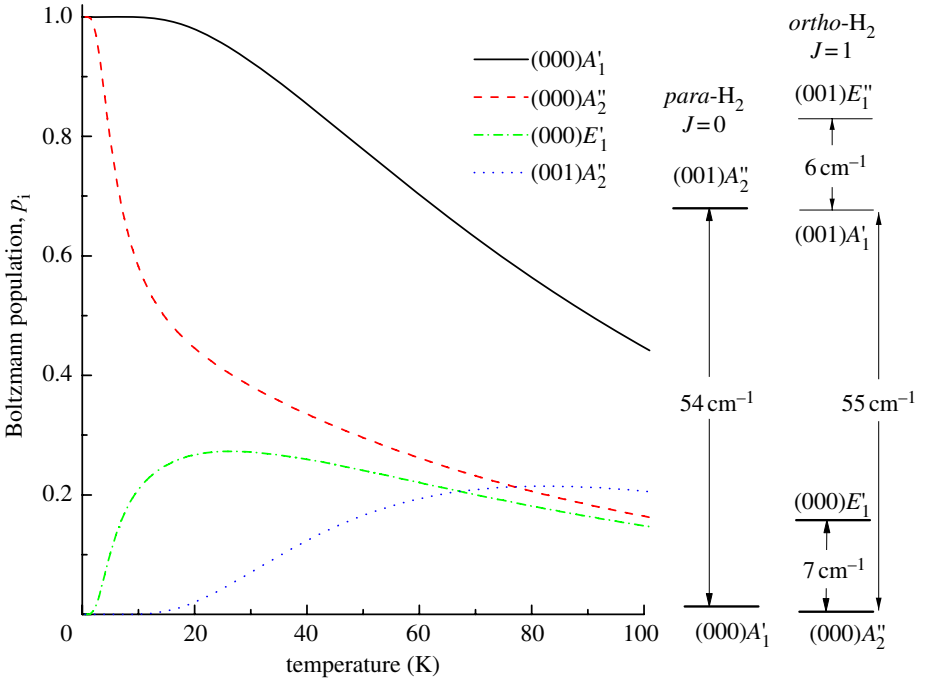

Figure 1. Boltzmann population of the $H_2@C_{70}$ *para* ground translational state (000)(solid line) and the first thermally excited (dotted line) state (001) and of the two *ortho* states A_2'' (dashed line) and E_1' (dashed-dotted line) in the ground translational state (000) calculated using energy levels of the five-dimensional quantum mechanical calculation [41] and equation (2.20) with $n_k = 1$; irreducible representations are from table 2. (Online version in colour.)

(d) Infrared absorption by $H_2@C_{70}$

The infrared absorption in $H_2@C_{70}$ is given by electric dipole operators d_0 and $d_{\pm1}$, which transform as A_2'' and E_1' irreducible representations of D_{5h}. At low temperature the symmetry-allowed transitions from the ground *para* state are $A_1' \xrightarrow{d_0} A_2''$ and $A_1' \xrightarrow{d_{\pm1}} E_1'$. Two *ortho* states, A_2'' and E_1', are populated at low temperature (figure 1). The transitions are $A_2'' \xrightarrow{d_0} A_1'$ and $A_2'' \xrightarrow{d_{\pm1}} E_1''$. The symmetry-allowed transitions from the E_1' state are $E_1' \xrightarrow{d_0} E_1''$ and $E_1' \xrightarrow{d_{\pm1}} A_1', A_2', E_2'$.

The IR absorption line area is proportional to the Boltzmann population of the initial state (equation (2.20)). The degeneracy g_j of the energy level E_j is one or two in the case of $H_2@C_{70}$. Figure 1 shows the Boltzmann population of the few first *para* and *ortho* levels in the $v = 0$ vibrational state. The *para* state (000) population (solid line) starts to drop above 20 K as the first excited state (001) (dotted line) at 54 cm^{-1} above the ground state becomes populated and drains the population from the (000) state. The abrupt change of the population of *ortho* ground states above 2 K is because of the transfer of population from the non-degenerate A_2'' ground level (dashed line) to the doubly degenerate E_1' (dashed-dotted line) 7 cm^{-1} higher. The populations of the A_2'' and E_1' states decrease above 30 K as the first excited translational (001) *ortho* state becomes more populated.

3. Experiment

The endohedral complexes were prepared by 'molecular surgery' as described in [11,12]; $H_2@C_{60}$, $D_2@C_{60}$ and $H_2@C_{70}$ at Kyoto University, Kyoto, Japan, and $HD@C_{60}$ at Kyoto University and Columbia University, New York, NY. The $HD@C_{60}$ sample was a mixture of the hydrogen isotopologues $H_2 : HD : D_2$ with the ratio 45 : 45 : 10. Since all C_{60} cages are filled, the filling factor

for HD is $\rho = 0.45$. The content of the C_{70} sample was empty : H_2 : $(H_2)_2 = 28 : 70 : 2$ and the filling factor $\rho = 0.7$. Experimental absorption spectra were corrected for the filling factor.

The *para*-enriched sample was made at Columbia University using molecular oxygen as a spin catalyst for the *ortho–para* conversion [26]. Briefly, the $H_2@C_{60}$ adsorbed on the external surface of NaY zeolite was immersed in liquid oxygen at 77 K for 30 min, thereby converting the incarcerated H_2 spin isomers to the equilibrium distribution at 77 K, $n_o/n_p = 1.0$. The liquid oxygen was pumped away and the endofullerene–NaY complex was brought back rapidly to room temperature. The *para*-enriched $H_2@C_{60}$ was extracted from the zeolite with CS_2 and the solvent was evaporated by argon. The powder sample under an argon atmosphere and on dry ice arrived at the National Institute of Chemical Physics and Biophysics, Tallinn, Estonia, 4 days after the preparation.

Powdered samples were pressed under vacuum into 3 mm diameter pellets for IR transmission measurements. Typical sample thickness was 0.3 mm. Two identical vacuum tight chambers with Mylar windows were employed in the IR measurements. The chambers were put inside an optical cold finger-type cryostat with KBr windows. During the measurements, the chamber containing the pellet for analysis was filled with He exchange gas while the empty chamber served as a reference. Transmission spectra were obtained using a Bruker interferometer Vertex 80 v with a halogen lamp and a HgCdTe or an InSb detector. The apodized resolution was typically 0.3 cm^{-1} or better.

Transmission $T_r(\omega)$ was measured as the light intensity transmitted by the sample divided by the light intensity transmitted by the reference. The absorption coefficient $\alpha(\omega)$ was calculated from the transmission $T_r(\omega)$ through $\alpha(\omega) = -d^{-1} \ln[T_r(\omega)(1-R)^{-2}]$, with the reflection coefficient $R = [(\eta-1)/(\eta+1)]^2$ calculated assuming a frequency-independent index of refraction [85], $\eta = 2$. Absorption spectra were cut into shorter pieces around groups of H_2 lines and a baseline correction was performed before fitting the H_2 lines with Gaussians.

4. Results and discussion

(a) H_2, D_2 and HD in C_{60}

The IR absorption spectra of $H_2@C_{60}$ at 6 K together with the simulated spectra are shown in figure 2 and the diagram of the energy levels involved is shown in figure 3*a*. The simulated spectra are calculated using Hamiltonian, dipole moment and the *ortho–para* ratio parameters (table 3) obtained from the fit of 200 K spectra [33]. Temperature does not affect these parameters and the line intensities follow the Boltzmann population of initial states [33]. The intensity of three lines, $Q(0)^0$ and $Q(1)^1$ in figure 2*a* and $S(1)^3$ in figure 2*c*, cannot be simulated because the induced dipole moment theory does not describe $\Delta N = 0$ transitions. However, the position of these three lines was used to fit the Hamiltonian parameters [33]. The intensity of the *ortho* state $N = J = 1$ into $\Lambda = 0, 1$ and 2 by translation–rotation coupling is seen in figure 2*b*. The *para* $N = 1, J = 2$ and *ortho* $N = 1, J = 3$ states are split into three sublevels as well. However, because of the selection rule $\Delta\Lambda = \pm 1$ only one *para* and one *ortho* *S*-transition is IR active.

The intensity of other lines in figure 2*b–d* is described accurately by two dipole moment parameters, A^{101} and A^{121}, and the *ortho–para* ratio $n_o/n_p = 2.89 \pm 0.045$, which is very close to the statistical value three (table 3). We confirmed the assignment of spectral lines to *para*- and *ortho*-H_2 by measuring the spectrum of a *para*-enriched $H_2@C_{60}$ sample [33]. Low-temperature spectra in the region of *Q* lines are shown in figure 4. The time delay between *para* enrichment and the first IR measurement was 4 days. The 4255 cm^{-1} *para* line is stronger and the other three *ortho* lines are weaker in the *para*-enriched sample than in the non-enriched sample.

Figure 4 deserves some attention. Lines $Q(0)^1$ and $Q(1)^0$ have a clear multi-component structure and it is different for the two samples. This is not possible in the approximation of spherical symmetry—not even by considering the true icosahedral symmetry of C_{60} because the lowest Λ value for the state which is split by the icosahedral symmetry is three while the initial and final states of the optical transitions under discussion only have $\Lambda = 0, 1$. Later measurements

Table 3. Values of the fitted parameters for $H_2@C_{60}$ [33] and for HD and $D_2@C_{60}$ [34]. The vibrational and rotational constants of a free molecule of the three hydrogen isotopologues are shown for comparison; gas-phase ω_0 is calculated including all terms $(v+\frac{1}{2})^k$ up to $k=3$ [86]. The parameter ${}^{v}V_{00}^{224}$ is set to zero for HD@C_{60} and $D_2@C_{60}$. Parameter errors are given in [34].

κ_i	$H_2@C_{60}$		HD@C_{60}		$D_2@C_{60}$		unit
	$v=0$	$v=1$	$v=0$	$v=1$	$v=0$	$v=1$	
${}^{v}V_{00}^{002}$	14.28	15.95	16.36	17.48	16.78	16.46	Jm^{-2}
${}^{v}V_{00}^{004}$	2.21×10^{21}	2.192×10^{21}	1.88×10^{21}	2.13×10^{21}	2.16×10^{21}	2.39×10^{21}	Jm^{-4}
${}^{v}V_{00}^{222}$	0.563	1.20	1.31	2.04	1.1	1.4	Jm^{-2}
${}^{v}V_{00}^{224}$	2.21×10^{20}	1.03×10^{20}	0	0	0	0	Jm^{-4}
${}^{v}V_{00}^{111}$	—	—	3.11×10^{-10}	3.25×10^{-10}	—	—	Jm^{-1}
${}^{v}V_{00}^{113}$	—	—	4.3×10^{10}	7.1×10^{10}	—	—	Jm^{-3}
n_o/n_p	2.89		—		2		
A^{010}	—		-1.5×10^{-32}		—		Cm
A^{101}	9.1×10^{-22}		7.0×10^{-22}		6.9×10^{-22}		C
A^{121}	-4.3×10^{-22}		-2.7×10^{-22}		-2.9×10^{-22}		C
κ_i	$H_2@C_{60}$	H_2	HD@C_{60}	HD	$D_2@C_{60}$	D_2	unit
ω_0	4062.4	4161.18	3549.7	3632.20	2924	2993.69	cm^{-1}
B_e	59.87	60.853	45.4	45.655	29.89	30.444	cm^{-1}
α_e	2.97	3.062	1.70	1.986	1.09	1.079	cm^{-1}
D_e	4.83×10^{-2}	4.71×10^{-2}	1.5×10^{-1}	2.605×10^{-2}	8×10^{-3}	1.141×10^{-2}	cm^{-1}

on the relaxed but initially *para* converted sample showed that the difference between the line shapes of the normal and *para* converted sample are not due to the different *ortho–para* ratio. Thus, it is likely that the difference in the line splitting is due to a different impurity content of the two samples. However, it is not completely excluded that the crystal field or the distortion of the C_{60} cage is responsible for part of this splitting. Note that the $Q(1)^0$ line in $D_2@C_{60}$ (figure 5) bears a similar splitting pattern to that in $H_2@C_{60}$.

The $D_2@C_{60}$ spectrum (figure 5) is shifted to a lower frequency than that of $H_2@C_{60}$ because of the heavier mass of D_2. The spectrum has fewer lines than the $H_2@C_{60}$ spectrum. The missing transitions in $D_2@C_{60}$ (table 4) belong to the *J*-odd species, which are in the minority for D_2.

The splitting of $N=J=1$ into $\Lambda=0,1$ and 2 states is similar in D_2 and H_2. The magnitude of the splitting, $\hbar\,{}^{v}\omega_0^{\mathrm{T}}(\sqrt{5}/20)({}^{v}V_{00}^{222}/{}^{v}V_{00}^{002})$ (table 1), is less in D_2 because ${}^{1}\omega_0^{\mathrm{T}}$ is smaller, although ${}^{1}V_{00}^{002}$ and ${}^{1}V_{00}^{222}$ are similar for the two isotopologues (table 3). Line $Q(1)^2$ overlaps partially with the $Q(0)^1$ line (figure 5). However, this is not because the translation–rotation splitting is different for the two isotopologues but because of a smaller anharmonic correction α_e of the rotational constant for D_2 (table 3).

The spectrum of HD@C_{60} is more simple (figure 6) because there are no *para* and *ortho* species and therefore only one state is populated at low temperature. There is one spectral line, not present in homonuclear dihydrogen, labelled $R(0)$ in figures 3*b* and 6. HD has no inversion symmetry and the ban on $\Delta J=1$ transitions is lifted. The classification of this transition as $\Delta J=1$ is arbitrary, first, because the weight of $JNL\Lambda=1201$ is only 0.5 in this state [34] and, second, the change of translational state is $\Delta N=2$, which is not allowed by any of the dipole operator components in our model. The next component in the final state is $JNL\Lambda=2111$ with weight 0.29, which makes this transition A^{121}-active, $N=0\rightarrow1$, $J=0\rightarrow2$, and therefore it would be more appropriate to classify it as an *S* line.

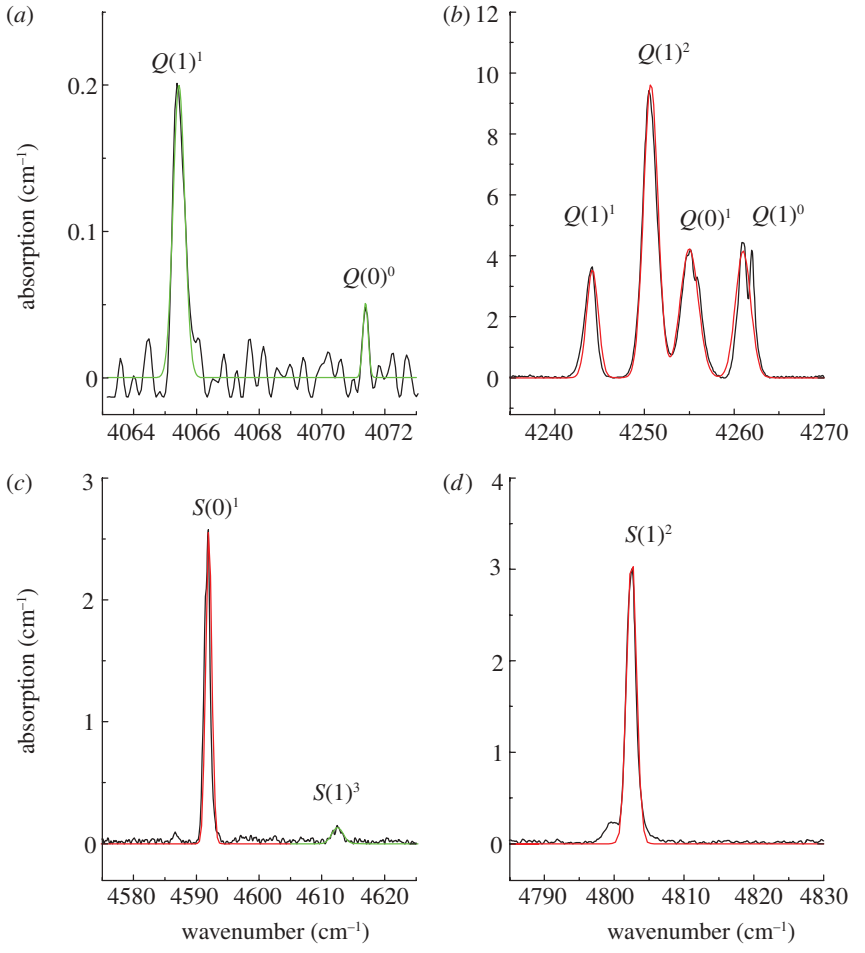

Figure 2. IR absorption spectra of $H_2@C_{60}$ at 6 K are shown by the black line. The green line in (*a*) is the Gaussian fit of fundamental *para* and *ortho* transitions, $\Delta N = \Delta J = 0$. The red line in (*b–d*) is the simulated spectrum with parameters taken from the model fit of 200 K spectra [33]. The $S(1)^3$ labelled green line in (*c*) is the Gaussian fit of the $\Delta N = 0$, $\Delta J = 2$ forbidden *ortho* transition, experimentally observed at 4612.5 cm^{-1} and predicted to be at 4613.1 cm^{-1} by our model [33]. Line labels are the same as in figure 3*a*; the superscript to the line label shows the final state Λ.

Another interesting feature of the HD spectrum is the absence of the $\Delta N = 0, \Delta J = 1$ ($0000 \rightarrow 1001$) transition, although the induced dipole moment coefficient A^{010} gives a two orders of magnitude larger dipole moment than the permanent dipole moment of free HD, as was discussed in [34]. This $\Delta J = 1$ transition in $HD@C_{60}$ is suppressed because there is an interference of two dipole terms, A^{010} and A^{101}, which have opposite signs. The final state consists of 80% of the pure rotational state $J = 1, N = 0$ and 18% of the pure translational state $N = 1, J = 0$. This mixed final state has matrix elements from the ground state for both A coefficients, A^{010} and A^{101}, which nearly cancel each other.

The observed low-temperature IR transitions of H_2, D_2 and $HD@C_{60}$ are collected in table 4. The content of the unperturbed $|JNL\Lambda\rangle$ state in the final state is above $|\xi^1|^2 = 0.9$ in homonuclear species in most cases, while for HD it varies and could be as low as 0.5. The mixing of states ξ^v is proportional to the energy separation of mixed states, $E_j - E_i$ in the first-order perturbation theory. F_{00}^{00} couples states where $L_i = L_j$ and $J_i = J_j$. These states are far from each other as $L_i = L_j$ only if $N_j = N_i \pm 2$. The other term F_{00}^{22} mixes $L_j = L_i \pm 2$ and $J_j = J_i \pm 2$, which are even further

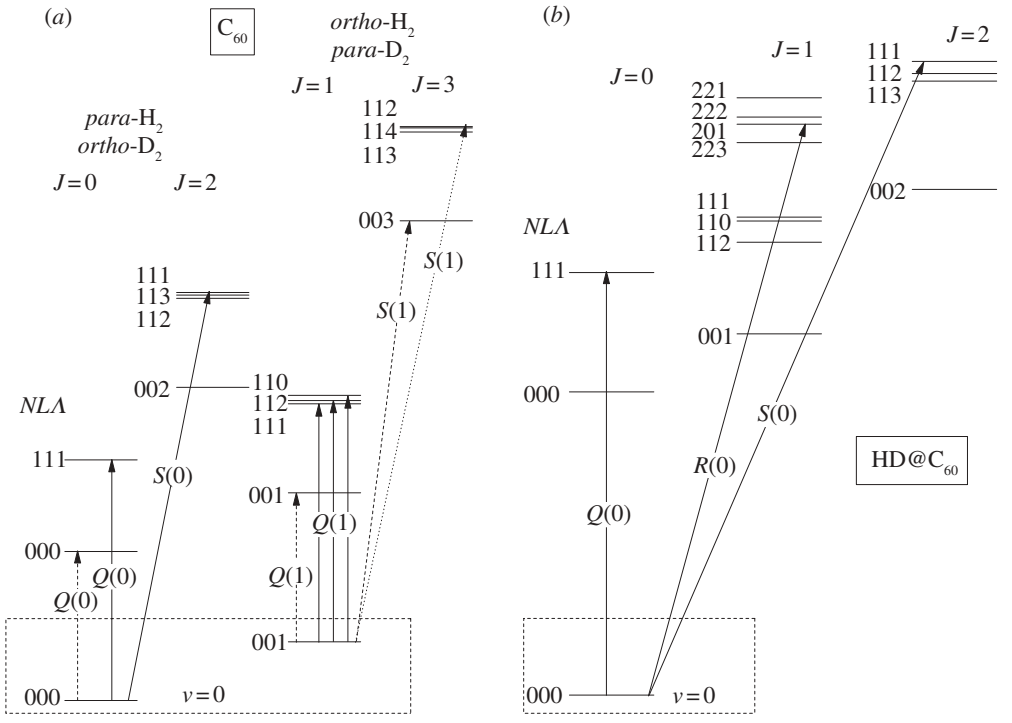

Figure 3. Diagrams of the observed low-temperature IR transitions in hydrogen isotopologues (*a*) H_2, D_2 and (*b*) HD incarcerated in C_{60}. The initial states surrounded by a dashed box have the vibrational quantum number $v = 0$; all the final states are in the excited vibrational state $v = 1$. Dashed lines in (*a*) are forbidden transitions ($\Delta N = 0$) that are observed in $H_2@C_{60}$ but not in $D_2@C_{60}$. The *S*(1) line (dotted) with $\Delta N = 1$ is not observed in $D_2@C_{60}$. The line label $Q(J_i)$ is used for $\Delta J = 0$, $R(J_i)$ is used for $\Delta J = +1$ and $S(J_i)$ for $\Delta J = +2$ transitions where J_i is the initial state *J*.

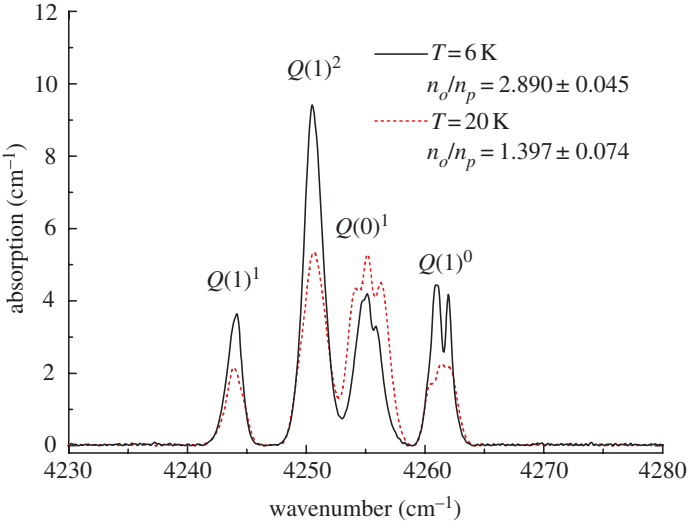

Figure 4. IR absorption spectra in the region of *Q* lines of a *para*-enriched $H_2@C_{60}$ (dashed line) and non-enriched sample (solid line) at low temperature (*T*). The thermal equilibrium *ortho–para* ratio at 77 K where the sample was *para* enriched is $n_o/n_p = 1.0$. (Online version in colour.)

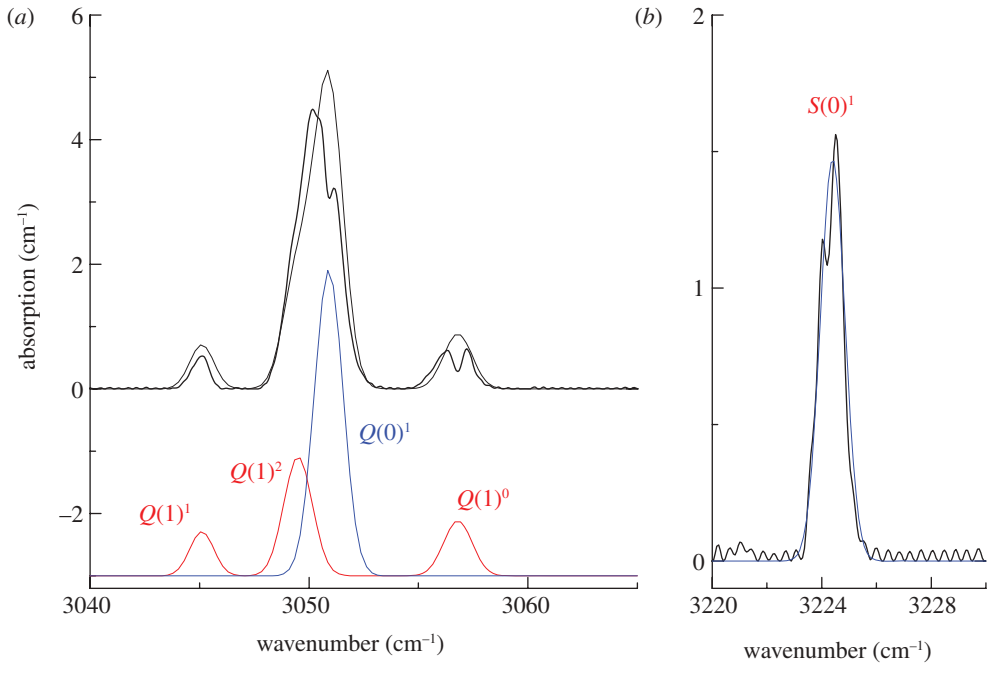

Figure 5. IR absorption spectra of D_2@C_{60} at 5 K. The simulated spectrum is shown by the red line (*para*), the blue line (*ortho*) and the thin black line (sum of *para* and *ortho* spectra). The parameters for the simulated spectrum are taken from the model fit of the 90 K spectrum [34]. Line labels are the same as in figure 3*a*; superscript to the line label shows the final state Λ.

Table 4. Experimental IR absorption line parameters of endohedral dihydrogen isotopologues in C_{60} at 5 K. ω is the transition frequency in wavenumber units, cm^{-1}, and S is the integrated absorption line area in cm^{-2} units. $JNL\Lambda$ are the quantum numbers of the main component with the weight $|\xi^1|^2$ in the final state $v = 1$. The $|\xi^0|^2$ of the main component $JNL\Lambda$ in the initial $v = 0$ state for H_2 is 0.97 of 0000 and 0.97 of 1001, for D_2 is 0.99 of 0000 and 0.99 of 1001, and for HD is 0.95 of 0000. Integrated absorption cross-section σ (unit: cm per molecule) is used by some authors, $\sigma = SV/\mathcal{N}$, where $\mathcal{N}$ is the number of hydrogen molecules in the volume V [87]; $\mathcal{N}/V = 1.48 \times 10^{21}$ cm^{-3} in solid C_{60}.

line	H_2			D_2			HD			$v = 1$
label	ω	S	$\lvert\xi^1\rvert^2$	ω	S	$\lvert\xi^1\rvert^2$	ω	S	$\lvert\xi^1\rvert^2$	$JNL\Lambda$
$Q(1)^1$	4065.4	0.093	0.98	—	—	0.99	—	—	0.80	1001
$Q(0)^0$	4071.4	0.011	0.98	—	—	0.99	—	—	0.96	0000
$Q(1)^1$	4244.5	5.76	0.95	3045.1	0.98	0.97	—	—	0.94	1111
$Q(1)^2$	4250.7	19.3	0.94	3050.2[a]	10.8	0.96	—	—	0.64	1112
$Q(0)^1$	4255.2	10.6	0.94	3050.2[a]	10.8	0.96	3710.8	23.5	0.73	0111
$Q(1)^0$	4261.0	8.86	0.94	3056.8	1.55	0.96	—	—	0.64	1110
$R(0)^1$	—	—	0.61	—	—	0.61	3906.7	1.05	0.50	1201
$S(0)^1$	4592.0	3.08	0.94	3224.35	1.66	0.96	3988.9	1.6	0.54	2111
$S(1)^1$	4612.5	0.3	0.97	—	—	0.96	—	—	0.58	3003
$S(1)^2$	4802.5	5.65	0.94	—	—	0.86	—	—	0.64	3112

[a]It was not possible to separate overlapping $Q(0)^1$ and $Q(1)^2$ lines of D_2 and the line area given is the sum of both transitions.

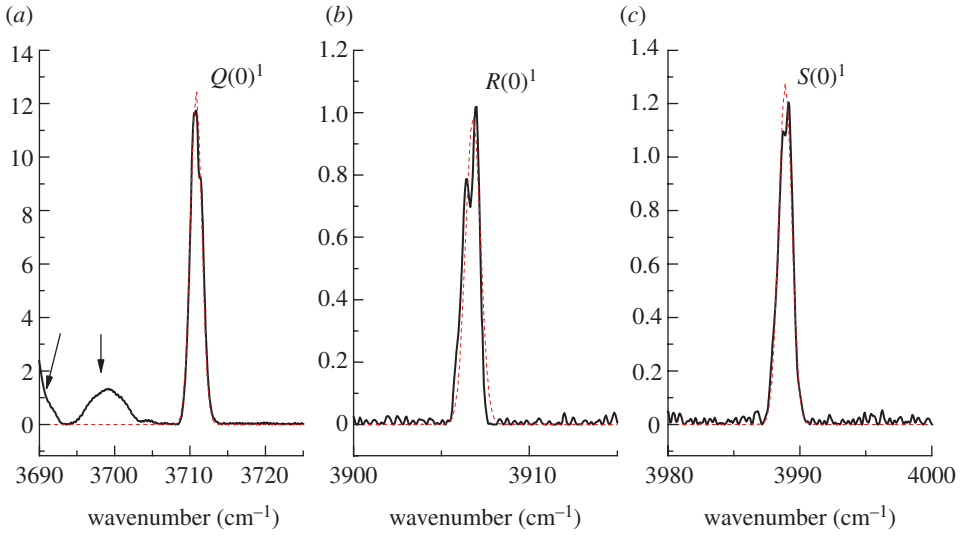

Figure 6. IR absorption spectra of HD@C_{60} at 5 K, black line. The parameters for the simulated spectrum (red dashed line) are taken from the model fit of 90 K spectra [34]. The broad lines indicated by arrows are not due to HD. Line labels are the same as in figure 3*b*; superscript to the line label shows the final state Λ. (Online version in colour.)

from each other for small N. It was found by Xu *et al.* [41] that J is almost a good quantum number in H_2 and D_2@C_{60} but not in HD@C_{60}. Indeed, the distance between mixed states decreases for HD as F^{11}_{00} mixes $L_j = L_i \pm 1$ and $J_j = J_i \pm 1$ and for this $N_j = N_i \pm 1$.

The vibrational frequency ω_0 is redshifted from its gas-phase value for H_2 and D_2 (table 3). The relative change in the frequency $[\omega_0(\text{gas}) - \omega_0(C_{60})]\omega_0(\text{gas})$ depends on the cage and is independent of the hydrogen isotopologue [88]. Based on our fit results (table 3), for H_2 $\omega_0(C_{60})/\omega_0(\text{gas}) = 0.9763$ and for HD $\omega_0(C_{60})/\omega_0(\text{gas}) = 0.9773$. We used the average of these two ratios to calculate the D_2@C_{60} fundamental vibrational frequency, $\omega_0 = 2924\ \text{cm}^{-1}$, that was necessary to fit the IR spectra to a model Hamiltonian [34]. At this point we cannot say how much of the redshift is caused by a change in the zero-point vibrational energy and how much is caused by the change of anharmonic corrections to the vibrational levels in the C_{60} as our dataset is limited to energy differences of $v = 0$ and 1 levels only. Note that the vibrational frequency of H_2@C_{60} is $\omega_0 = 4062.4\ \text{cm}^{-1}$ (table 3), while the *para* vibrational transition is shifted up by $9\ \text{cm}^{-1}$, to $\omega_0 = 4071.4\ \text{cm}^{-1}$ (table 4). This is because the zero-point translational energies are different in the $v = 0$ and 1 vibrational states [33].

The rotational constant B_e, the vibrational correction α_e, and the centrifugal correction D_e of the hydrogen inside C_{60} and in free space are compared in table 3. The smaller than the gas-phase value of B_e may be interpreted as 0.8% (0.9%) stretching of the nucleus–nucleus distance s in H_2@C_{60} (D_2@C_{60}), as $B_e \sim \langle 1/s^2 \rangle$. An attractive interaction between hydrogen atoms and the cage causes s to be longer. The elongation of the equilibrium proton–proton distance is consistent with the redshift of ω_0 [89]. However, the anharmonic vibrational correction to the rotational constant, α_e, is smaller inside the cage than in the gas phase. Here, the cage has the opposite, repulsive, effect and reduces the elongation of the proton–proton distance in the excited v states when compared with H_2 in the free space. This is supported by the fact that within the error bars α_e of D_2@C_{60} is equal to α_e of D_2. The vibrational amplitude of D_2 is less than that of the H_2 and therefore the repulsive effect of the cage becomes important at $v > 1$ for D_2.

Among the rotational and vibrational constants of HD@C_{60} the centrifugal correction D_e to the rotational constant is anomalously different from its gas-phase value compared with the other two isotopologues (table 3). Positive D_e means that the faster the molecule rotates, the longer is the

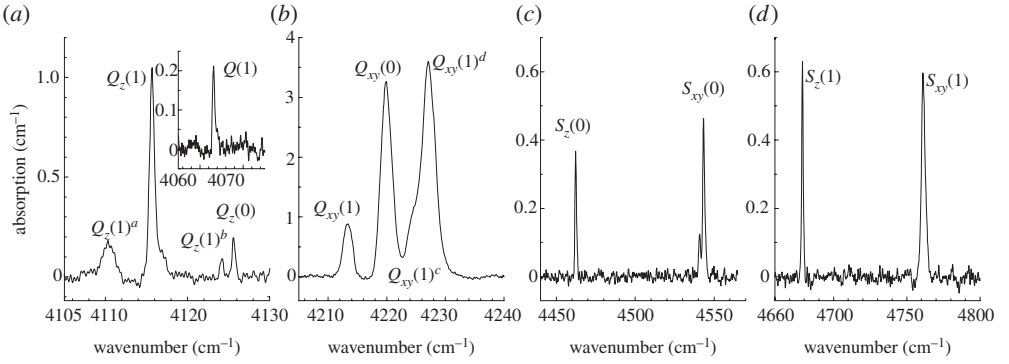

Figure 7. IR absorption spectra of $H_2@C_{70}$ at 5 K. The line labels (table 5) refer to the z (xy) mode transition where $Q_z(J)$ [$Q_{xy}(J)$] is the $\Delta n_z = 1$, $\Delta J = 0$ [$\Delta n = 1$, $\Delta J = 0$] and $S_z(J)$ [$S_{xy}(J)$] is the $\Delta n_z = 1$, $\Delta J = 2$ [$\Delta n = 1$, $\Delta J = 2$] transition; J is the initial state rotational quantum number. Inset to (*a*) shows the pure vibrational *ortho*-H_2 transition without the change of translational or rotational state.

bond. We speculate that, since the rotation centre of HD inside the cage is further away from the deuteron, the centrifugal force on the deuteron increases and the bond is stretched more than in the free HD molecule.

A similar system to the one studied here is exohedral H_2 in C_{60}. There, H_2 occupies the octahedral interstitial site in the C_{60} crystal. The prominent features in the exohedral H_2 IR spectra [56] are the translational, $\Delta N = \pm 1$, sidebands to the fundamental transitions, $\Delta v = 1$ and $\Delta J = 0, 2$. The redshift of the fundamental vibrational frequency is about 60 cm^{-1}, which is less than in $H_2@C_{60}$, where it is 98.8 cm^{-1}. Also, the separation of the translational $N = 0$ and 1 levels, approximately 120 cm^{-1}, is less than that in $H_2@C_{60}$, 184.4 cm^{-1}. It is likely that the main contribution to the latter difference comes from the larger van der Waals volume available for H_2 in the octahedral site than in the C_{60} cage.

(b) $H_2@C_{70}$

IR absorption spectra of $H_2@C_{70}$ measured at 5 K are shown in figure 7, and the scheme of energy levels with the low-temperature transitions indicated with arrows is shown in figure 8. The transitions where $\Delta J = 0$ and the translational state changes by $\Delta n = 1$ or $\Delta n_z = 1$ are labelled as $Q_{xy}(J)$ and $Q_z(J)$, where J is the rotational quantum number of the initial state. The transitions where $\Delta J = 2$ are labelled by $S_{xy}(J)$ and $S_z(J)$. The z and xy translational modes have distinctly different energies. For the Q lines they are shown in different panels (figure 7*a*,*b*). The *para* and *ortho* S lines are well separated because of different rotational energies. The *para* S lines are shown in figure 7*c*, whereas *ortho* S lines are shown in figure 7*d*. The Q lines cannot be sorted out into *para* and *ortho* that easily. An exception is the $Q(1)$ transition, inset to figure 7*a*. This is a pure vibrational transition, $v = 0 \rightarrow 1$, without the change of translational or rotational states. The corresponding (fundamental) *para* transition $Q(0)$ would be at 4069.3 cm^{-1} according to the model (table 5). We expect it to be much weaker than the *ortho* $Q(1)$ transition, as in $H_2@C_{60}$, and for this reason it is not observed in the experiment.

In figure 9, we plot the normalized line area and normalized Boltzmann population. Figure 9*a* shows the temperature dependence of *para* lines. The assignment of the 4125.6 cm^{-1} line to $Q_z(0)$ and the 4219.9 cm^{-1} line to $Q_{xy}(0)$ is supported by our model, which is summarized in table 5 and will be discussed below.

The uniaxial symmetry of C_{70} splits the *ortho* ground state $J = 1$. This splitting is about 7 cm$^{-1} \approx 10$ K and creates a sharp temperature dependence of the *ortho* line intensity at low temperature as is shown in figure 1. This feature could be used to determine which of the Q

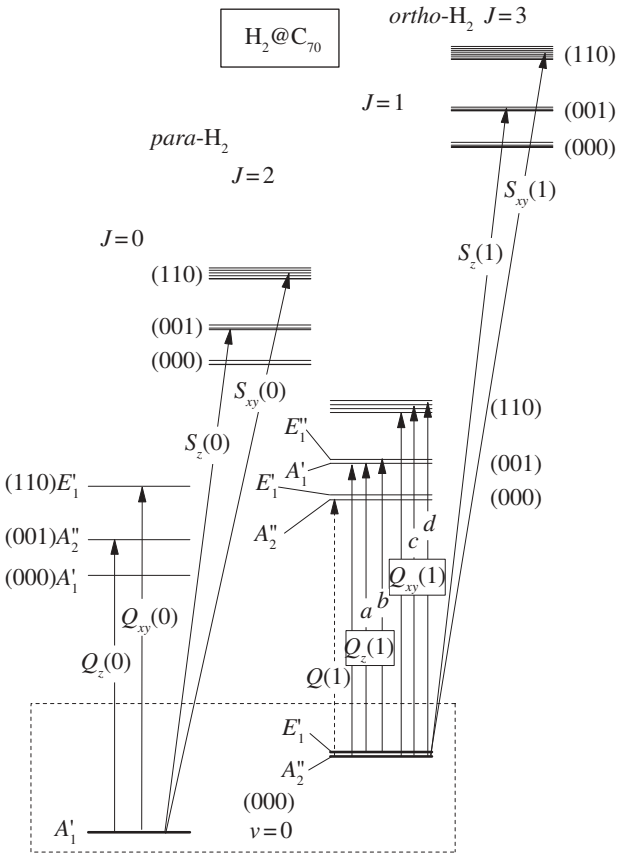

Figure 8. Energy levels and observed IR transitions of $H_2@C_{70}$ from the ground *para* and *ortho* translational states in the $\upsilon = 0$ state to the excited vibrational state $\upsilon = 1$. The irreducible representations of the symmetry group D_{5h} (table 2) are given for a few lower states. The ordering of the states is based on [41]. *Ortho*-H_2 transitions marked by *a* and *b* are $Q_z(1)^a$ and $Q_z(1)^b$ in table 5 and start from the thermally excited state, which is E_1' (000) according to Xu *et al*. [41]. There are three experimentally observed *ortho*-H_2 transitions from the ground A_2'' (000) state: $Q_{xy}(1)$, $Q_{xy}(1)^c$ and $Q_{xy}(1)^d$.

lines belong to the *ortho* species. Two lines, 4110.3 cm^{-1} and 4124.2 cm^{-1}, have a temperature dependence consistent with the *ortho* transitions starting from the ground translational (000) state of E_1' symmetry (figure 9*c*). However, according to our model, there is no transition close to 4124.2 cm^{-1} from the thermally excited *ortho* E_1' state (table 5). This might be due to our simplified model, where the rotational anisotropy parameter ${}^{\upsilon}\kappa$ is assumed equal in the $\upsilon = 0$ and 1 vibrational states. The rest of the *ortho* lines are shown in figure 9*b*. Several lines follow the same temperature dependence, the fundamental transition at 4063.2 cm^{-1}, $Q_{xy}(1)$ lines 4213.4, 4224.2 and 4227.2 cm^{-1} and the $S_z(1)$ line at 4678.8 cm^{-1}. Lines $Q_z(1)$ at 4115.7 and $S_{xy}(1)$ at 4761.3 cm^{-1} have distinctly different temperature dependence from the rest of the lines. Such deviation could be due to the overlap of transitions starting from A_2'' *and* E_1' symmetry states. However, none of the *ortho* lines behaves like the theoretical prediction (black line) so the possibility that the ground *ortho* state is doubly degenerate E_1' and not the A_2'', i.e. ${}^0\kappa < 0$, is not ruled out by our data. The dashed black line shows the ground-state population if the ground state is E_1' and the A_2'' state is 7 cm^{-1} above it. This temperature dependence is closer to the experimental situation than the solid black line, where ${}^0\kappa > 0$. The change of sign of ${}^0\kappa$ affects the temperature dependence of intensities only a little if the transitions start from the thermally excited state, as shown in figure 9*c*, where the red dashed line is the normalized Boltzmann population of the A_2'' state *if* this state is 7 cm^{-1} above the ground state E_1', i.e. if ${}^0\kappa < 0$.

Table 5. IR transitions of $H_2@C_{70}$ observed at 5 K from the vibrational state $\upsilon = 0$ to the state $\upsilon = 1$. $J(nln_z)$ are the quantum numbers for the initial and final states and the labels indicate corresponding transitions in figures 7 and 8. The experimental spectra were fitted with Gaussians, S_{exp} is the experimental line area; the experimental line position ω_{exp} could always be determined with a precision better than 0.1 cm^{-1}. The model parameters, equation (2.14), were determined as described in the text by setting the model frequency ω_{mod} equal to the experimental frequency ω_{exp} for four lines indicated with error **0**. The model parameters are vibrational frequency $\omega_0 = 4069.1\ cm^{-1}$, one-dimensional oscillator frequency along the z-axis ${}^{\upsilon}\omega_z^{\mathrm{T}} = 56.5\ cm^{-1}$, two-dimensional circular oscillator frequency ${}^{\upsilon}\omega_{xy}^{\mathrm{T}} = 150.9\ cm^{-1}$ and the rotational anisotropy parameter ${}^{\upsilon}\kappa = 3.1\ cm^{-1}$. The rotational constant $B_e = 59.865\ cm^{-1}$ and its corrections, $\alpha_e = 2.974\ cm^{-1}$ and $D_e = 0.04832\ cm^{-1}$, were assumed to be the same as in $H_2@C_{60}$.

frequency (cm^{-1})			initial $\upsilon = 0$		final $\upsilon = 1$			error (cm^{-1})
ω_{exp}	ω_{mod}	S_{exp} (cm^{-2})	J	(nln_z)	J	(nln_z)	label	$\omega_{exp} - \omega_{mod}$
4063.2	4063.2	0.146 ± 0.005	1	(000)	1	(000)	$Q(1)$	**0**
—	4069.1	—	0	(000)	1	(000)	$Q(0)$	—
4110.3	4110.3	0.311 ± 0.014	1	(000)	1	(001)	$Q_z(1)^a$	**0**
4115.7	4119.7	0.824 ± 0.009	1	(000)	1	(001)	$Q_z(1)$	−4.0
4124.2	4119.7	0.045 ± 0.007	1	(000)	1	(001)	$Q_z(1)^b$	4.5
4125.6	4125.6	0.096 ± 0.007	0	(000)	0	(001)	$Q_z(0)$	**0**
4213.3	4214.1	1.759 ± 0.024	1	(000)	1	(110)	$Q_{xy}(1)$	−0.8
4220.0	4220.0	7.702 ± 0.027	0	(000)	0	(110)	$Q_{xy}(0)$	**0**
4224.2	4214.1	2.111 ± 0.066	1	(000)	1	(110)	$Q_{xy}(1)^c$	10.1
4227.2	4214.1	10.143 ± 0.067	1	(000)	1	(110)	$Q_{xy}(1)^d$	13.1
4462.3	4456.3	0.570 ± 0.023	0	(000)	2	(001)	$S_z(0)$	6.0
4543.4	4550.7	0.582 ± 0.012	0	(000)	2	(110)	$S_{xy}(0)$	−7.3
4678.8	4667.0	0.831 ± 0.012	1	(000)	3	(001)	$S_z(1)$	11.8
4761.3	4761.3	1.900 ± 0.019	1	(000)	3	(110)	$S_{xy}(1)$	0

It is not unreasonable that ${}^{0}\kappa < 0$ and the E_1' ($J_z = \pm 1$) state is the ground rotational state of *ortho*-H_2. It requires that there is an attraction instead of repulsion between H and C when H_2 is in the centre of the C_{70} cage. The attraction is stronger for the H_2 if its molecular axis is in the xy plane, $J_z = \pm 1$, where the distance between H and C is less than if the axis is along the z plane, $J_z = 0$, where the H–C distance is longer. Indeed, the attraction between C and H in $H_2@C_{60}$ was deduced from the redshift of vibrational energy and reduced rotational constant compared with H_2 in the gas phase [33]. However, it was found by five-dimensional quantum mechanical calculation that A_2'' is the ground state [41]. A more elaborate model with dipole moment parameters that describe the IR line intensities together with the Boltzmann population could resolve the issue.

Table 5 summarizes the assignment of transitions observed in the experiment. Since our model described in §2*b* did not include translation–rotation coupling we used the transitions where both L and J are zero or one of them is zero in the initial and final states. The fundamental frequency $\omega_0 = 4069.1\ cm^{-1}$ was chosen to match the experimental fundamental *ortho* transition $Q(1)$; the rotational constant $B_e = 59.865\ cm^{-1}$ and its corrections $\alpha_e = 2.974\ cm^{-1}$, $D_e = 0.04832\ cm^{-1}$ for $H_2@C_{60}$ were used. Next the two *para* transitions were matched, $Q_z(0)$ and $Q_{xy}(0)$, to obtain ${}^{\upsilon}\omega_z^{\mathrm{T}} = 56.5\ cm^{-1}$, ${}^{\upsilon}\omega_{xy}^{\mathrm{T}} = 150.9\ cm^{-1}$. The 4220 cm^{-1} line was chosen as $Q_{xy}(0)$ because its temperature dependence (figure 9*a*) is similar to the $S_z(0)$ and $S_{xy}(0)$ line temperature dependence. The *ortho* ground-state splitting is 9.4 cm^{-1} (7.4 cm^{-1} from the five-dimensional calculation [41]) with

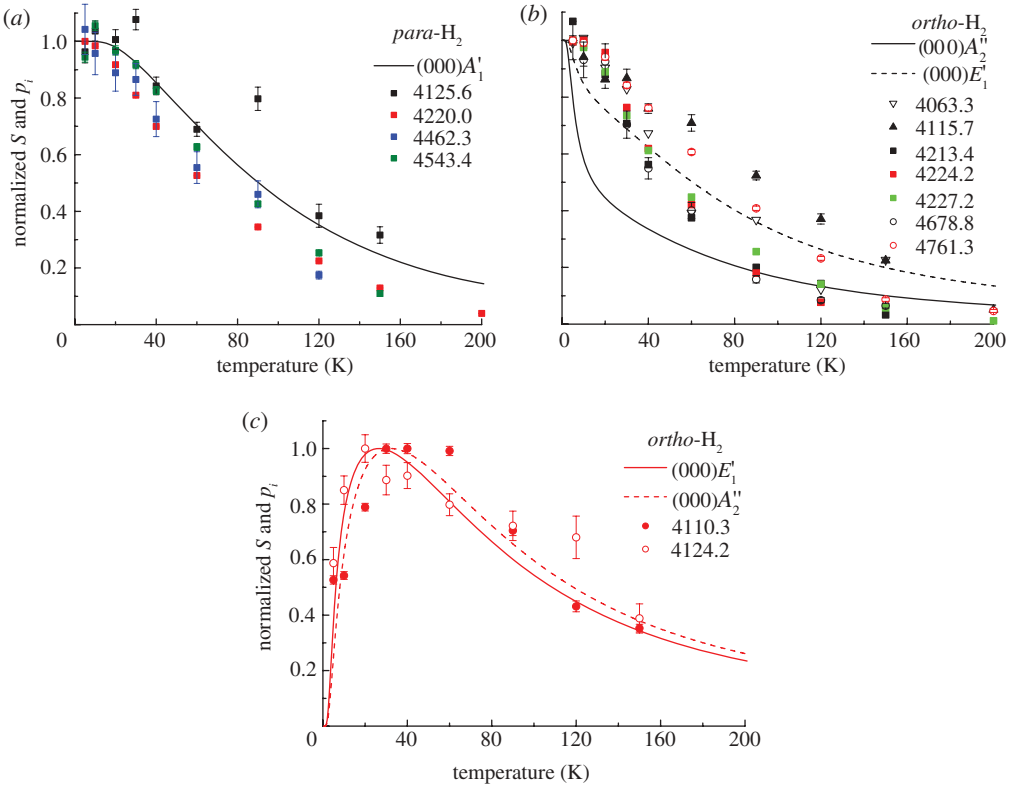

Figure 9. Normalized line area and Boltzmann population of *para* and *ortho* transitions of $H_2@C_{70}$ starting from the ground translational state. (*a*) *para* lines; (*b*) and (*c*) *ortho* lines. Solid line in (*b*) is the normalized intensity when the initial state is the ground state A_2'' ($J_z = 0$) and in (*c*) when the initial state is E_1' ($J_z = \pm 1$), 7 cm^{-1} above A_2''. This corresponds to ${}^{v}\kappa > 0$, equation (2.13). Dashed line in (*b*) and (*c*) is the reverse situation when the ground state is doubly degenerate E_1' and A_2'' is 7 cm^{-1} above it, i.e. ${}^{v}\kappa < 0$. The normalized intensities are calculated using the translational energy levels from the five-dimensional quantum mechanical calculation [41] and equation (2.20).

${}^{v}\kappa = 3.1\,cm^{-1}$, which was obtained by assuming that the $Q_z(1)^a$ transition, $(000)E_1' \rightarrow (001)A_1'$ in figure 8, is centred at 4110.3 cm^{-1}. It was assumed that the anharmonic corrections to translational energy and to ${}^{v}\kappa$ are same for the $v = 0$ and $v = 1$ vibrational states.

The variation in the experimental frequencies compared with the model frequencies is within $\pm 10\,cm^{-1}$ (table 5). This is reasonable since our model did not include translation–rotation coupling, and the translation–rotation coupling in $H_2@C_{60}$ creates splittings of this magnitude. The vibrational frequency ω_0 is larger in $H_2@C_{70}$ than in $H_2@C_{60}$. This difference should not be overinterpreted, because the correction owing to the difference in zero-point translational energies in two vibrational states was not taken into account for $H_2@C_{70}$, as was done for $H_2@C_{60}$ [33]. Again, a more elaborate model is needed for C_{70} than the two-oscillator model described in §2*b*.

5. Conclusions

IR absorption spectra of endohedral hydrogen isotopologues H_2 [32,33], D_2 [34] and HD [34] in C_{60} are informative, involving excitations of vibrations, rotations and translational motion of dihydrogen. The translational motion of the encapsulated molecule is quantized and coupled to its rotations because of the surrounding C_{60} cage. The vibrational frequency of dihydrogen is redshifted compared with the gas-phase value. Together with the smaller rotational constant it

shows that the hydrogen bond is stretched inside the cage and there is an attraction between H (or D) and C. The heteronuclear HD does not rotate about its centre of mass because of the surrounding cage. Different rotational and translational states are mixed and rotational quantum number J is not a good quantum number for HD@C_{60}.

Our study shows that the vibrations and rotations of C_{60} and the crystal field effects of solid C_{60} are not important on the energy scale of IR measurements. If these effects are important their contribution to the IR spectra is of the order of one wavenumber splitting of a few absorption lines. Such small splitting is consistent with the NMR [28,29] and heat capacity [30] results.

C_{70} has an ellipsoidal shape and this splits the translation–rotation states of H_2. The translational frequency is about 180 cm^{-1} in H_2@C_{60}. In C_{70}, this three-dimensional mode is split into a two-dimensional mode at 151 cm^{-1} and a one-dimensional mode at 56 cm^{-1}. The five-dimensional quantum mechanical calculation [41] is in very good agreement with this experimental result.

Funding statement. This research was supported by the Estonian Ministry of Education and Research, grant SF0690029s09, and by the Estonian Science Foundation, grant nos. ETF8170, ETF8703 and JD187.

References

1. Kroto HW, Heath JR, O'Brian SC, Curl RF, Smalley RE. 1985 C_{60}: buckminsterfullerene. *Nature* **318**, 162–163. (doi:10.1038/318162a0)
2. Heath JR, O'Brien SC, Zhang Q, Liu Y, Curl RF, Tittel FK, Smalley RE. 1985 Lanthanum complexes of spheroidal carbon shells. *J. Am. Chem. Soc.* **107**, 7779–7780. (doi:10.1021/ja00311a102)
3. Saunders M, Jiménez-Vázquez HA, Cross RJ, Poreda RJ. 1993 Stable compounds of helium and neon: He@C_{60} and Ne@C_{60}. *Science* **259**, 1428–1430. (doi:10.1126/science.259.5100.1428)
4. Saunders M, Jiménez-Vázquez HA, Cross RJ, Mroczkowski S, Gross ML, Giblin DE, Poreda RJ. 1994 Incorporation of helium, neon, argon, krypton, and xenon into fullerenes using high pressure. *J. Am. Chem. Soc.* **116**, 2193–2194. (doi:10.1021/ja00084a089)
5. Mauser H, Hirsch A, van Eikema Hommes NJR, Clark T, Pietzak B, Weidinger A, Dunsch L. 1997 Stabilization of atomic nitrogen inside C_{60}. *Angew. Chem. Int Ed.* **36**, 2835–2838. (doi:10.1002/anie.199728351)
6. Larsson JA, Greer JC, Harneit W, Weidinger A. 2002 Phosphorous trapped within buckminsterfullerene. *J. Chem. Phys.* **116**, 7849–7854. (doi:10.1063/1.1468643)
7. Dunsch L, Yang S. 2007 Metal nitride cluster fullerenes: their current state and future prospects. *Small* **3**, 1298–1320. (doi:10.1002/smll.200700036)
8. Rubin Y. 1997 Organic approaches to endohedral metallofullerenes: cracking open or zipping up carbon shells? *Chem. Eur. J.* **3**, 1009–1016. (doi:10.1002/chem.19970030705)
9. Rubin Y, Jarrosson T, Wang GW, Bartberger MD, Houk KN, Schick G, Saunders M, Cross RJ. 2001 Insertion of helium and molecular hydrogen through the orifice of an open fullerene. *Angew. Chem. Int. Ed.* **40**, 1543–1546. (doi:10.1002/1521-3773(20010417)40:8<1543::AID-ANIE1543>3.0.CO;2-6)
10. Murata Y, Murata M, Komatsu K. 2003 100% Encapsulation of a hydrogen molecule into an open-cage fullerene derivative and gas-phase generation of H_2@C_{60}. *J. Am. Chem. Soc.* **125**, 7152–7153. (doi:10.1021/ja0354162)
11. Komatsu K, Murata M, Murata Y. 2005 Encapsulation of molecular hydrogen in fullerene C_{60} by organic synthesis. *Science* **307**, 238–240. (doi:10.1126/science.1106185)
12. Murata M, Murata Y, Komatsu K. 2006 Synthesis and properties of endohedral C_{60} encapsulating molecular hydrogen. *J. Am. Chem. Soc.* **128**, 8024–8033. (doi:10.1021/ja061857k)
13. Murata Y, Maeda S, Murata M, Komatsu K. 2008 Encapsulation and dynamic behavior of two H_2 molecules in an open-cage C_{70}. *J. Am. Chem. Soc.* **130**, 6702–6703. (doi:10.1021/ja801753m)
14. Murata M, Maeda S, Morinaka Y, Murata Y, Komatsu K. 2008 Synthesis and reaction of fullerene C_{70} encapsulating two molecules of H_2. *J. Am. Chem. Soc.* **130**, 15800–15801. (doi:10.1021/ja8076846)
15. Iwamatsu S, Stanisky CM, Cross RJ, Saunders M, Mizorogi N, Nagase S, Murata S. 2006 Carbon monoxide inside an open-cage fullerene. *Angew. Chem. Int. Ed.* **45**, 5337–5340. (doi:10.1002/anie.200601241)

16. Iwamatsu SI, Uozaki T, Kobayashi K, Re S, Nagase S, Murata S. 2004 A bowl-shaped fullerene encapsulates a water into the cage. *J. Am. Chem. Soc.* **126**, 2668–2669. (doi:10.1021/ja038537a)
17. Xiao Z *et al.* 2007 Synthesis of [59]fullerenones through peroxide-mediated stepwise cleavage of fullerene skeleton bonds and X-ray structures of their water-encapsulated open-cage complexes. *J. Am. Chem. Soc.* **129**, 16 149–16 162. (doi:10.1021/ja0763798)
18. Whitener KE, Frunzi M, Iwamatsu SI, Murata S, Cross RJ, Saunders M. 2008 Putting ammonia into a chemically opened fullerene. *J. Am. Chem. Soc.* **130**, 13996–13999. (doi:10.1021/ja805579m)
19. Whitener KE, Cross RJ, Saunders M, Iwamatsu SI, Murata S, Mizorogi N, Nagase S. 2009 Methane in an open-cage$_{60}$ fullerene. *J. Am. Chem. Soc.* **131**, 6338–6339. (doi:10.1021/ja901383r)
20. Kurotobi K, Murata Y. 2011 A single molecule of water encapsulated in fullerene C_{60}. *Science* **333**, 613–616. (doi:10.1126/science.1206376)
21. Beduz C *et al.* 2012 Quantum rotation of ortho and para-water encapsulated in a fullerene cage. *Proc. Natl Acad. Sci. USA* **109**, 12 894–12 898. (doi:10.1073/pnas.1210790109)
22. Sartori E, Ruzzi M, Turro NJ, Decatur JD, Doetschman DC, Lawler RG, Buchachenko AL, Murata Y, Komatsu K. 2006 Nuclear relaxation of H_2 and H_2@C_{60} in organic solvents. *J. Am. Chem. Soc.* **128**, 14752–14753. (doi:10.1021/ja065172w)
23. Chen JYC, Marti AA, Turro NJ, Komatsu K, Murata Y, Lawler RG. 2010 Comparative NMR properties of H_2 and HD in toluene-d8 and in H_2/HD@C_{60}. *J. Phys. Chem. B.* **114**, 14 689–14 695. (doi:10.1021/jp102860m)
24. Sartori E, Ruzzi M, Turro NJ, Komatsu K, Murata Y, Lawler RG, Buchachenko AL. 2008 Paramagnet enhanced nuclear relaxation of H_2 in organic solvents and in H_2@C_{60}. *J. Am. Chem. Soc.* **130**, 2221–2225. (doi:10.1021/ja076071g)
25. Frunzi M, Lei X, Murata Y, Komatsu K, Iwamatsu SI, Murata S, Lawler RG, Turro NJ. 2010 Magnetic interaction of solution-state paramagnets with encapsulated H_2O and H_2. *J. Phys. Chem. Lett.* **1**, 1420–1422. (doi:10.1021/jz100336x)
26. Turro NJ *et al.* 2008 Demonstration of a chemical transformation inside a fullerene. The reversible conversion of the allotropes of H_2@C_{60}. *J. Am. Chem. Soc.* **130**, 10506–10507. (doi:10.1021/ja804311c)
27. Frunzi M *et al.* 2011 A photochemical on–off switch for tuning the equilibrium mixture of H_2 nuclear spin isomers as a function of temperature. *J. Am. Chem. Soc.* **133**, 14 232–14 235. (doi:10.1021/ja206383n)
28. Carravetta M, Johannessen OG, Levitt MH, Heinmaa I, Stern R, Samoson A, Horsewill AJ, Murata Y, Komatsu K. 2006 Cryogenic NMR spectroscopy of endohedral hydrogen–fullerene complexes. *J. Chem. Phys.* **124**, 104507. (doi:10.1063/1.2174012)
29. Carravetta M *et al.* 2007 Solid-state NMR of endohedral hydrogen–fullerene complexes. *Phys. Chem. Chem. Phys.* **9**, 4879–4894. (doi:10.1039/b707075f)
30. Kohama Y *et al.* 2009 Rotational sublevels of an ortho-hydrogen molecule encapsulated in an isotropic C_{60} cage. *Phys. Rev. Lett.* **103**, 073001. (doi:10.1103/PhysRevLett.103.073001)
31. Mamone S, Chen JYC, Bhattacharyya R, Levitt MH, Lawler RG, Horsewill AJ, Rõõm T, Bačić Z, Turro NJ. 2011 Theory and spectroscopy of an incarcerated quantum rotor: the infrared spectroscopy, inelastic neutron scattering and nuclear magnetic resonance of H_2@C_{60} at cryogenic temperature. *Coord. Chem. Rev.* **255**, 938–948. (doi:10.1016/j.ccr.2010.12.029)
32. Mamone S *et al.* 2009 Rotor in a cage: infrared spectroscopy of an endohedral hydrogen-fullerene complex. *J. Chem. Phys.* **130**, 081103. (doi:10.1063/1.3080163)
33. Ge M *et al.* 2011 Interaction potential and infrared absorption of endohedral H_2 in C_{60}. *J. Chem. Phys.* **134**, 054507. (doi:10.1063/1.3535598)
34. Ge M *et al.* 2011 Infrared spectroscopy of endohedral HD and D_2 in C_{60}. *J. Chem. Phys.* **135**, 114511. (doi:10.1063/1.3637948)
35. Horsewill AJ *et al.* 2010 Inelastic neutron scattering of a quantum translator–rotator encapsulated in a closed fullerene cage: isotope effects and translation–rotation coupling in H_2@C_{60} and HD@C_{60}. *Phys. Rev. B* **82**, 081410. (doi:10.1103/PhysRevB.82.081410)
36. Rafailov PM, Thomsen C, Bassil A, Komatsu K, Bacsa W. 2005 Inelastic light scattering of hydrogen containing open-cage fullerene ATOCF. *Phys. Status Solidi A* **242**, R106–R108. (doi:10.1002/pssb.200541168)
37. Brown JM, Carrington A. 2003 *Rotational spectroscopy of diatomic molecules.* Cambridge, UK: Cambridge University Press.

38. Turro NJ *et al.* 2010 The spin chemistry and magnetic resonance of $H_2@C_{60}$. From the Pauli principle to trapping a long lived nuclear excited spin state inside a buckyball. *Acc. Chem. Res.* **43**, 335. (doi:10.1021/ar900223d)
39. Xu M, Sebastianelli F, Bačić Z, Lawler R, Turro NJ. 2008 Quantum dynamics of coupled translational and rotational motions of H_2 inside C_{60}. *J. Chem. Phys.* **128**, 011101. (doi:10.1063/1.2828556)
40. Xu M, Sebastianelli F, Bačić Z, Lawler R, Turro NJ. 2008 H_2 , HD, and D_2 inside C_{60}: coupled translation–rotation eigenstates of the endohedral molecules from quantum five-dimensional calculations. *J. Chem. Phys.* **129**, 064313. (doi:10.1063/1.2967858)
41. Xu M, Sebastianelli F, Gibbons BR, Bačić Z, Lawler R, Turro NJ. 2009 Coupled translation–rotation eigenstates of H_2 in C_{60} and C_{70} on the spectroscopically optimized interaction potential: effects of cage anisotropy on the energy level structure and assignments. *J. Chem. Phys.* **130**, 224306. (doi:10.1063/1.3152574)
42. Lee TB, McKee ML. 2008 Endohedral hydrogen exchange reactions in C_{60} ($nH_2@C_{60}, n = 1 - 5$): comparison of recent methods in a high-pressure cooker. *J. Am. Chem. Soc.* **130**, 17 610–17 619. (doi:10.1021/ja8071868)
43. Sebastianelli F, Xu M, Bačić Z, Lawler R, Turro NJ. 2010 Hydrogen molecules inside fullerene C_{70}: quantum dynamics, energetics, maximum occupancy, and comparison with C_{60}. *J. Am. Chem. Soc.* **132**, 9826–9832. (doi:10.1021/ja103062g)
44. Erkol H, Demiralp E. 2009 Exact solutions for a Hamiltonian with the Morse potential and the Dirac delta shell interactions. *Mol. Phys.* **107**, 2053–2062. (doi:10.1080/00268970903140441)
45. Dolgonos GA, Peslherbe GH. 2011 Conventional and density-fitting local Møller–Plesset theory calculations of C_{60} and its endohedral $H_2@C_{60}$ and $2H_2@C_{60}$ complexes. *Chem. Phys. Lett.* **513**, 236–240. (doi:10.1016/j.cplett.2011.08.002)
46. Jiménez-Osés G, Garciá JI, Corzana F, Elguero J. 2011 Accurate calculation of chemical shifts in highly dynamic $H_2@C_{60}$ through an integrated quantum mechanics/molecular dynamics scheme. *Org. Lett.* **13**, 2528–2531. (doi:10.1021/ol2004116)
47. Shaffer WH. 1944 Degenerate modes of vibration and perturbations in polyatomic molecules. *Rev. Mod. Phys.* **16**, 245–259. (doi:10.1103/RevModPhys.16.245)
48. Flügge S. 1971 *Practical quantum mechanics*, vol. 1. Berlin, Germany: Springer.
49. Cross RJ. 2001 Does H_2 rotate freely inside fullerenes? *J. Phys. Chem. A* **105**, 6943. (doi:10.1021/jp011054d)
50. Yildirim T, Harris AB. 2002 Rotational and vibrational dynamics of interstitial molecular hydrogen. *Phys. Rev. B* **66**, 214301. (doi:10.1103/PhysRevB.66.214301)
51. Krause M, Hulman M, Kuzmany H, Dubay O, Kresse G, Vietze K, Seifert G, Wang C, Shinohara H. 2004 Fullerene quantum gyroscope. *Phys. Rev. Lett.* **93**, 137403. (doi:10.1103/PhysRevLett.93.137403)
52. Michel KH, Verberck B, Hulman M, Kuzmany H, Krause M. 2007 Superposition of quantum and classical rotational motions in $Sc_2C_2@C_{84}$ fullerite. *J. Chem. Phys.* **126**, 064304. (doi:10.1063/1.2434175)
53. Smith AP, Benedek R, Trouw FR, Minkoff M, Yang LH. 1996 Quasi-two-dimensional quantum states of H_2 in stage-2 Rb-intercalated graphite. *Phys. Rev. B* **53**, 10187–10199. (doi:10.1103/PhysRevB.53.10187)
54. Bengtsson L, Svensson K, Hassel M, Bellman J, Persson M, Andersson S. 2000 H_2 adsorbed in a two-dimensional quantum rotor state on a stepped copper surface. *Phys. Rev. B* **61**, 16 921–16 932. (doi:10.1103/PhysRevB.61.16921)
55. FitzGerald SA, Forth S, Rinkoski M. 2002 Induced infrared absorption of molecular hydrogen in solid C_{60}. *Phys. Rev. B* **65**, 140302. (doi:10.1103/PhysRevB.65.140302)
56. FitzGerald SA, Churchill HOH, Korngut PM, Simmons CB, Strangas YE. 2006 Low-temperature infrared spectroscopy of H_2 in crystalline C_{60}. *Phys. Rev. B* **73**, 155409. (doi:10.1103/PhysRevB.73.155409)
57. Kolesnikov AI, Antonov VE, Bashkin IO, Grosse G, Moravsky AP, Muzychka AY, Ponyatovsky EG, Wagner FE. 1997 Neutron spectroscopy of C_{60} fullerite hydrogenated under high pressure; evidence for interstitial molecular hydrogen. *J. Phys. Condens. Matter.* **9**, 2831. (doi:10.1088/0953-8984/9/13/022)
58. FitzGerald SA, Yildirim T, Santodonato LJ, Neumann DA, Copley JRD, Rush JJ, Trouw F. 1999 Quantum dynamics of interstitial H_2 in solid C_{60}. *Phys. Rev. B.* **60**, 6439–6451. (doi:10.1103/PhysRevB.60.6439)

59. Tomaselli M, Meier BH. 2001 Rotational-state selective spectra of hydrogen in a molecular trap. *J. Chem. Phys.* **115**, 11017. (doi:10.1063/1.1429655)
60. Tomaselli M. 2003 Dynamics of diatomic molecules confined in a chemical trap. I. Nuclear magnetic resonance experiments on hydrogen in solid C_{60}. *Mol. Phys.* **101**, 3029–3051. (doi:10.1080/00268970310001627431)
61. Williams KA, Pradhan BK, Eklund PC, Kostov MK, Cole MW. 2002 Raman spectroscopic investigation of H_2, HD, and D_2 physisorption on ropes of single-walled, carbon nanotubes. *Phys. Rev. Lett.* **88**, 165502. (doi:10.1103/PhysRevLett.88.165502)
62. Herman RM, Lewis JC. 2006 Theory of the fundamental vibration–rotation–translation spectrum of H_2 in a C_{60} lattice. *Phys. Rev. B* **73**, 155408. (doi:10.1103/PhysRevB.73.155408)
63. Olthof EHT, van der Avoird A, Wormer PES. 1996 Vibration and rotation of CO in C_{60} and predicted infrared spectrum. *J. Chem. Phys.* **104**, 832–847. (doi:10.1063/1.470809)
64. Cohen-Tannoudji C, Diu B, Laloë F. 1977 *Quantum mechanics.* Paris, France: Wiley-VCH.
65. Herzberg G. 1950 *Molecular spectra and molecular structure. I. Spectra of diatomic molecules*, 2nd edn. Princeton, NJ: Van Nostrand Company, Inc.
66. Dunham JL. 1932 The energy levels of a rotating vibrator. *Phys. Rev.* **41**, 721–731. (doi:10.1103/PhysRev.41.721)
67. Altmann SL, Herzig P. 1994 *Point-group theory tables*. Oxford, UK: Oxford University Press.
68. Gordy W, Cook RL. 1984 *Microwave molecular spectra*, 3rd edn. Techniques of Chemistry, no. 18. New York, NY: Wiley-Interscience.
69. Hedberg K, Hedberg L, Bühl M, Bethune DS, Brown CA, Johnson RD. 1997 Molecular structure of free molecules of the fullerene C_{70} from gas-phase electron diffraction. *J. Am. Chem. Soc.* **119**, 5314–5320. (doi:10.1021/ja970110e)
70. Hedberg K, Hedberg L, Bethune DS, Brown CA, Dorn HC, Johnson RD, de Vries M. 1991 Bond lengths in the free molecules of buckminsterfullerene, C_{60}, from gas-phase electron diffraction. *Science* **254**, 410. (doi:10.1126/science.254.5030.410)
71. Yildirim T, Harris AB. 2003 Quantum dynamics of a hydrogen molecule confined in a cylindrical potential. *Phys. Rev. B* **67**, 245413. (doi:10.1103/PhysRevB.67.245413)
72. Allin EJ, Hare WFJ, MacDonald RE. 1955 Infrared absorption of liquid and solid hydrogen. *Phys. Rev.* **98**, 554–555. (doi:10.1103/PhysRev.98.554)
73. Hare WFJ, Allin EJ, Welsh HL. 1955 Infrared absorption of liquid and solid hydrogen with various ortho-para ratios. *Phys. Rev.* **99**, 1887–1888. (doi:10.1103/PhysRev.99.1887)
74. Hourahine B, Jones R. 2003 Infrared activity of hydrogen molecules trapped in Si. *Phys. Rev. B.* **67**, 121205. (doi:10.1103/PhysRevB.67.121205)
75. Kudian AK, Welsh ML. 1971 Spectra of H_2-Ar, H_2-Kr, and H_2-Xe Van der Waals complexes in pressure-induced infrared absorption. *Can. J. Phys.* **49**, 230–242. (doi:10.1139/p71-025)
76. McKellar ARW, Welsh HL. 1974 Spectra of $(H_2)_2$, $(D_2)_2$, and H_2D_2 Van der waals complexes. *Can. J. Phys.* **52**, 1082–1089.
77. Chen EE, Stavola M, Fowler WB, Walters P. 2002 Key to understanding interstitial H_2 in Si. *Phys. Rev. Lett.* **88**, 105507. (doi:10.1103/PhysRevLett.88.105507)
78. Oka T. 1993 High-resolution spectroscopy of solid hydrogen. *Annu. Rev. Phys. Chem.* **44**, 299–333. (doi:10.1146/annurev.pc.44.100193.001503)
79. Frommhold L. 1993 *Collisison-induced absorption in gases.* Cambridge Monographs on Atomic, Molecular, and Chemical Physics, no. 2. Cambridge, UK: Cambridge University Press.
80. Berns RM, Wormer PES, Mulder F, van der Avoird A. 1978 Ab initio calculations of the collision-induced dipole in He–H_2. I. A valence bond approach. *J. Chem. Phys.* **69**, 2102–2109. (doi:10.1063/1.436810)
81. Wormer PES, Dijk GV. 1979 Ab initio calculations of the collision-induced dipole in He–H_2. II. SCF results and comparison with experiment. *J. Chem. Phys.* **70**, 5695–5702. (doi:10.1063/1.437447)
82. Meyer W, Frommhold L. 1986 Collision-induced rototranslational spectra of H_2-He from an accurate ab initio dipole moment surface. *Phys. Rev. A* **34**, 2771–2779. (doi:10.1103/PhysRevA.34.2771)
83. Frommhold L, Meyer W. 1987 Collision-induced rotovibrational spectra of H_2-He pairs from first principles. *Phys. Rev. A* **35**, 632–638. (doi:10.1103/PhysRevA.35.632)
84. Gustafsson M, Frommhold L, Meyer W. 2000 Infrared absorption spectra by H_2–He collisional complexes: the effect of the anisotropy of the interaction potential. *J. Chem. Phys.* **113**, 3641–3650. (doi:10.1063/1.1287822)

85. Homes CC, Horoyski PJ, Thewalt MLW, Clayman BP. 1994 Anomalous splitting of the $F_{1u}(\rightarrow 3F_u)$ vibrations in single-crystal C_{60} below the orientational-ordering transition. *Phys. Rev. B* **49**, 7052–7055. (doi:10.1103/PhysRevB.49.7052)
86. Huber KP, Herzberg G. 1979 *Constants of diatomic molecules*. Molecular Spectra and Molecular Structure, no. IV. New York, NY: Van Nostrand Reinhold Company.
87. Loudon R. 1983 *The quantum theory of light*, 2nd edn. London, UK: Oxford University Press.
88. Buckingham AD. 1960 Solvent effects in vibrational spectroscopy. *Trans. Faraday Soc.* **56**, 753–760. (doi:10.1039/tf9605600753)
89. Van de Walle CG. 1998 Energetics and vibrational frequencies of interstitial H_2 molecules in semiconductors. *Phys. Rev. Lett.* **80**, 2177–2180. (doi:10.1103/PhysRevLett.80.2177)